HOKKAIDO UNIVERSITY

Title	Different micro/nano-scale patterns of surface materials influence osteoclastogenesis and actin structure
Author(s)	Akasaka, Tsukasa; Tamai, Miho; Yoshimura, Yoshitaka; Ushijima, Natsumi; Numamoto, Shinichiro; Yokoyama, Atsuro; Miyaji, Hirofumi; Takata, Ryo; Yamagata, Shuichi; Sato, Yoshiaki; Nakanishi, Ko; Yoshida, Yasuhiro
Citation	Nano research, 15, 4201-4211 https://doi.org/10.1007/s12274-021-4026-3
Issue Date	2022-01-17
Doc URL	http://hdl.handle.net/2115/87800
Rights	This version of the article has been accepted for publication, after peer review (when applicable) and is subject to Springer Nature ' s AM terms of use, but is not the Version of Record and does not reflect post-acceptance improvements, or any corrections. The Version of Record is available online at: http://dx.doi.org/10.1007/s12274-021-4026-3
Type	article (author version)
File Information	Akasaka2022.pdf

Instructions for use

Hokkaido University Collection of Scholarly and Academic Papers : HUSCAP

Graphical Table of Contents

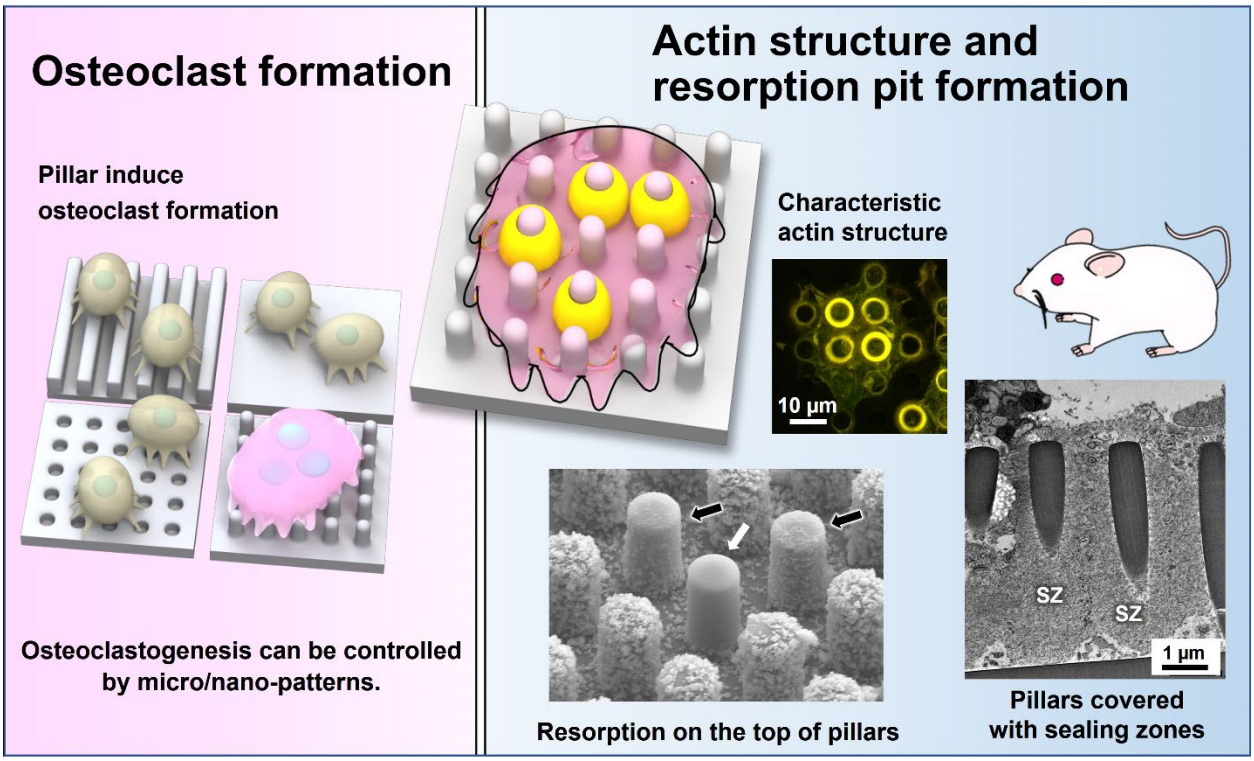

"Optimal surface patterns for inducing osteoclastogenesis and characteristic actin structures on pillars were found."

Different micro/nano-scale patterns of surface materials influence osteoclastogenesis and actin structure

Tsukasa Akasaka[1*], Miho Tamai[2], Yoshitaka Yoshimura[3], Natsumi Ushijima[4], Shinichiro Numamoto[5], Atsuro Yokoyama[5], Hirofumi Miyaji[6], Ryo Takata[7], Shuichi Yamagata[7], Yoshiaki Sato[7], Ko Nakanishi[1], and Yasuhiro Yoshida[1]

[1] *Department of Biomaterials and Bioengineering, Faculty of Dental Medicine, Hokkaido University, Sapporo 060-8586, Japan*

[2] *Immune Signal Unit, Okinawa Institute of Science and Technology Graduate University, Okinawa 904-0495, Japan*

[3] *Department of Pharmacology, Faculty of Dental Medicine and Graduate School of Dental Medicine, Hokkaido University, Sapporo 060-8586, Japan*

[4] *Support Section for Education and Research, Faculty of Dental Medicine, Hokkaido University, Sapporo 060-8586, Japan*

[5] *Oral Functional Prosthodontics, Division of Oral Functional Science, Faculty of Dental Medicine, Hokkaido University, Sapporo 060-8586, Japan*

[6] *Department of Periodontology and Endodontology, Faculty of Dental Medicine, Hokkaido University, Sapporo 060-8586, Japan*

[7] *Department of Orthodontics, Faculty of Dental Medicine and Graduate School of Dental Medicine, Hokkaido University, Sapporo 060-8586, Japan*

*Corresponding author: akasaka@den.hokudai.ac.jp

ABSTRACT

The surface topography of a material can influence osteoclast activity. However, the surface structural factors that promote osteoclast activity have not yet been investigated in detail. Therefore, we investigated osteoclastogenesis by testing various defined patterns with different dimensions and shapes. The systematic patterns, made of a cyclo-olefin polymer, were prepared at a micron-, submicron-, and nano-scale with a groove, hole, or pillar shape with a 1:1 pitch ratio. RAW264.7 cells were cultured on these patterns in the presence of the receptor activator of NF-κB ligand (RANKL). Osteoclast formation was induced in the order pillar > groove ≥ hole. The two-dimensional factors also indicated that submicron-sized patterns strongly induced osteoclast formation. The optimal pillar dimension for osteoclast formation was 500 nm in diameter and 2 μm in height. Furthermore, we observed two types of characteristic actin structure, i.e., belt-like structures with small hollow circles and isolated ring-like structures, that formed on or around the pillars depending on size and height. Furthermore, resorption pits were observed mainly on the top of calcium phosphate-coated pillars. Thus, osteoclasts prefer convex shapes, such as pillars for differentiation and resorption. Our results indicate that osteoclastogenesis can be controlled by designing surfaces with specific morphologies.

Keywords: Micro/nano-pattern, pillar, RAW264.7, osteoclast, actin structure, resorption pit

1 Introduction

The balance between bone resorption by osteoclasts and bone formation by osteoblasts relies on controlled bone tissue remodeling. Osteoclasts, which differentiate from the monocyte-

macrophage lineage, resorb bone and are important in regulating bone formation, especially of defective bone or around implants because they cooperate with osteoblasts and influence resorption of bone replacement materials [1, 2]. However, abnormal osteoclast activity is implicated in diseases such as osteolysis, osteoporosis, osteopetrosis, Paget's disease of bone, and inflammatory arthritis [3].

Previous studies have suggested that osteoclasts may sense surface topography [4–14]. Indeed, osteoclastic resorption activity is influenced by several factors [4–7], one of which is surface topography. Geblinger et al. [8] raised the possibility that bone surface features, such as sub-micrometer cracks, can stimulate local osteoclast resorptive activity. Shemesh et al. [9] reported that osteoclasts sealing zone rings preferentially develop around several micron-scale protrusions of bone slices. In contrast to active interactions with protrusions, osteoclasts do not preferentially interact with negative topography, such as osteocyte lacunae, microcracks, and microscratches, on bone and dentin slices [9, 10]. Nevertheless, the relationship between osteoclastogenesis and surface topography of the bone remains unclear.

The surface topography of materials used as a replacement for defective bone parts influences osteoclastic activity. Some bone replacement materials are typically regulated by surface roughness or porosity at the nano, submicron, or micron scale. Osteoclast formation and function was found to be influenced by the surface topography of grain-fused beta-tricalcium phosphate disks [11], hydroxyapatite (HA)-coated polycaprolactone (PLC) disks [12], biomimetic HA substrates [10], porous HA disks with grain-fused surfaces [13], and sandblasted titanium surfaces [14]. In many cases, submicron-scale rough surfaces were found to induce osteoclastic formation and function, with nanoscale and microscale rough surfaces having the opposite effect [11–13, 15]. However, submicron surface topography-induced osteoclastic formation and function differed from the topographic scale effect in other related studies on bone replacement materials, which

showed that osteoclastic activity was influenced by topography in a complicated manner [4, 10, 14, 16]. Thus, the optimal topography for osteoclast formation and function has not been fully elucidated because of structural irregularities in the surface topological substrates regulated by surface roughness or porosity.

Osteoclast formation and function on defined patterns (e.g., pillars, holes, grooves) with different structural factors at the microscopic or nanoscopic level have not been examined in detail [17–23]. These patterns can be fabricated through several methods such as nanoimprinting, micro-molding, laser ablation, and self-assembly [24–27], and their bioactivities have been widely investigated because they are known to influence cell attachment, proliferation, and differentiation [28–32]. Our previous study reported that osteoclast formation from RAW264.7 cells is slightly improved on hole patterns on glycol-modified polyethylene terephthalate film with a diameter of 500 nm and a depth of 500 nm [18]. The same has been reported regarding osteoclast formation or function on microgrooves [17], submicron-scale holes [18], nano-pillars [20], and concentric circular microgrooves [19]. Therefore, the induction or attenuation of osteoclastogenesis on defined patterns is dependent on pattern size, shape, and composition.

In the present study, we investigated the effect of different structural factors of defined patterns on osteoclast formation and function. Systematic micron-, submicron-, and nano-scale patterns of grooves, holes, or pillars with a 1:1 pitch ratio were prepared by heating and pressing cyclo-olefin polymer (COP) films. We used the macrophage cell line RAW264.7 in the presence of the receptor activator of NF-κB ligand (RANKL) as an *in vitro* cell culture system to assess osteoclast formation on the different patterns. Actin structure and pit formation by osteoclast-like cells derived from RAW264.7 cells were also investigated. Furthermore, actin structure on pillars was evaluated using a rat femoral implant model.

2 Experimental

2.1 Preparation of COP patterns

Patterned COP films were prepared via thermal nanoimprinting as previously reported [33]. The advantages of COP include precision molding ability for thermal nanoimprinting [34, 35], non-toxicity, stability in cell culture medium, and controllable wettability from by plasma treatment. Briefly, a silicon master mold containing grooves, holes, and pillars 4 × 4 mm^2 or 5 × 5 mm^2 in area were obtained from Kyodo International, Inc. (Kawasaki, Japan). The mold pattern dimensions included grooves/ridges and pillars with widths or diameters of 2 μm, 1 μm, or 500 nm and a height of 500 nm; holes with diameters of 2 μm, 1 μm, or 500 nm and a depth of 500 nm, 1 μm, or 2 μm; deeper holes with diameters of 50, 10, 5, and 1 μm and a depth of 10 or 5 μm; deeper groove with a width of 5 μm and a depth of 10 μm; and higher pillar with a diameter of 5 μm and a height of 10 μm. A silicon mold with an area of 10 × 10 mm^2 and a nano-scale hole with a diameter of 100 nm and a depth of 200 nm was provided by Sousei Hall at Hokkaido University though the Nanotechnology Platform Japan program. All patterns were designed as a 1:1 pitch ratio pattern. To transfer mold patterns to film, a COP film (ZF14-188; 188 μm thickness; ZEON Corp., Tokyo, Japan) was pressed onto the master mold using a heating press (AH-1TC; ASONE Co., Osaka, Japan) at 175 °C for 4 min under 2 MPa. The resulting patterned film was carefully peeled off from the mold. To regulate surface wettability, the patterned films were treated with low-pressure air plasma in a desktop vacuum plasma-generating device (45 W, YHS-R; Sakigake-Semiconductor Co., Kyoto, Japan) for 0, 1, 4, or 60 s. These plasma irradiation times were adopted upon considering the relationship between irradiation time and contact angle on the planar surface.

Briefly, the contact angles were set by considering similar intervals selected, as indicative from hydrophobicity to hydrophilicity (contact angle for the planar surface: 94° for 0 s, 69° for 1 s, 46° for 4 s, and 38° for 60 s) to avoid troublesome procedures due to the high number of samples used. To stabilize the wettability of the surface, patterned films were stored exposed to air for 1 week. The patterned films were then fixed in 3.5 cm tissue culture polystyrene (TCPS) dishes (AGC Techno Glass Co., Shizuoka, Japan) and sterilized using UV irradiation prior to performing biological assays.

2.2 Characterization of the surface patterns

Surface morphology was observed by scanning electron microscopy (SEM; S-4000; Hitachi High-Tech Fielding Co., Tokyo, Japan) after the surface of the patterned COP film was coated with Pt-Pd using an ion-sputtering device (E-1030; Hitachi High-Tech Fielding Co.). Contact angles of the patterns were measured after 1 week of plasma treatment, which was conducted to stabilize the surface properties. Ultra-pure water (0.5 μL; Kanto Chemical Co., Inc., Tokyo, Japan) was dropped onto the surface at 25 °C and 21% humidity for 10 s, after which images of the spreading water were acquired using a contact angle meter (DMs-200; Kyowa Interface Science Co., Saitama, Japan) [36].

2.3 Osteoclastogenic differentiation

Osteoclast formation on patterned COP films in the presence of RANKL was performed using an osteoclastogenic differentiation assay with RAW264.7 macrophages (TIB-71TM; American Type Culture Collection, Manassas, VA, USA), using a modified version of a previously reported protocol [18]. Briefly, frozen RAW264.7 cells were incubated in Dulbecco's modified Eagle's medium (Sigma-Aldrich, St. Louis, MO, USA) supplemented with 10% fetal bovine serum (FBS;

CELLect Silver; MP Biomedicals, Santa Ana, CA, USA) for 1 day. The attached RAW264.7 cells were scraped, collected, and seeded at a density of 6,000 cells/cm^2 on the patterns fixed in 3.5 cm TCPS. The cells were then cultured in 2 mL of α-minimum essential medium (Gibco, Waltham, MA, USA) supplemented with 10% FBS, 1% penicillin-streptomycin-amphotericin B suspension, and 10 ng/mL recombinant soluble RANKL (sRANKL; Oriental Yeast Co., Tokyo, Japan) at 37 °C in a 5% CO_2 humidified atmosphere for 6 days. The medium was changed every 2 days.

To confirm osteoclast formation, osteoclasts were identified by tartrate-resistant acid phosphatase (TRAP) staining and nuclei counting [18, 37]. TRAP activity is a histochemical marker of osteoclasts. Briefly, RAW264.7 cells were cultured under osteoclastic differentiation conditions. After 6 days of culturing, the cells were stained using a TRAP staining kit (Cosmo Bio Co., Tokyo, Japan) according to manufacturer's instructions. For clear nuclei counting, cells were stained in 2 mL deionized water containing 30 μL 4′,6-diamidino-2-phenylindole (DAPI) solution (1 mg/mL; Dojindo Laboratories, Kumamoto, Japan). The TRAP- and DAPI-stained cells were imaged under the bright field and fluorescence modes, respectively, of an all-in-one fluorescence microscope (BZ-9000; Keyence Corp., Osaka, Japan). TRAP-positive multinucleated cells were counted in random four fields over a total area of 11.2 mm^2 for each pattern; TRAP-positive multinucleated cells with > 3 nuclei were counted as osteoclasts.

2.4 SEM of cell morphology

To determine the morphology of cells growing on different patterns, the cultured cells were rinsed with phosphate-buffered saline (PBS) and fixed in 2.5% glutaraldehyde solution for 2 h. The specimens were dehydrated in a graded ethanol series (50%, 60%, 70%, 80%, 90%, 95%,

99.5%, and 100%) for 5 min each. The specimens were then subjected to critical-point drying, after which dried cells on the patterns were coated by Pt-Pd sputtering and observed using SEM.

2.5 Immunofluorescence staining

Immunofluorescence staining was performed as previously described [33]. Briefly, after 6 days of cell culture with 10 ng/mL sRANKL on pillar patterns (or 100 ng/mL sRANKL on groove and hole patterns with a height or depth of 10 μm), the cells were fixed in 4% paraformaldehyde in PBS for 5 min, followed by incubation with 0.5% Triton X-100 in PBS for 10 min and blocking with 1% bovine serum albumin (BSA) in PBS for 30 min. The cells were then stained with Acti-stain 555 fluorescent phalloidin (1:166; Cytoskeleton Inc., Denver, CO, USA), anti-vinculin Alexafluor 488 (1:83; eBioscience, San Diego, CA, USA), and/or 3 μL DAPI solution (1 mg/mL; Dojindo Laboratories) in 0.5 mL of 1% BSA in PBS, and incubated overnight at 4 °C. Finally, the cells were washed three times with PBS and mounted using ProLong Diamond Antifade Mounting Reagent (Thermo Fisher Scientific, Waltham, MA, USA).

Typical two-dimensional (2D) cytoskeletons of the cells were observed under a fluorescence microscope (BZ-9000) while 3D cytoskeletons were observed using confocal laser scanning microscopy (CLSM; Leica TCS SP8, Leica Microsystems, Wentzler, Germany). Images of serial sections along the Z-axis were acquired at 0.3 μm intervals; these Z-stacks were then processed using the Leica Application Suite X v3.4 software. The Z-stack images were then re-sliced to generate cross-sectional images.

2.6 Pit formation assay

Resorption of calcium phosphate (CaP) by osteoclasts on the patterned films was assessed using a pit formation assay with CaP-coated substrates [38, 39]. Pillars, grooves, and holes with a diameter or width of 5 μm and a height of 10 μm were treated with 120 s of plasma to facilitate CaP deposition. To deposit CaP, the plasma-treated patterns were immersed in 5 mL of Hank's balanced salt solution (Lonza Japan, Tokyo, Japan) and incubated at 37 °C for 5 days [40]; the solution was changed every two days. The resulting CaP-coated patterns were washed with water, dried, and fixed on 3.5 cm TCPS and sterilized using UV irradiation. Pit formation assays were performed under the culture conditions described for the osteoclastic differentiation assay. RAW264.7 cells were cultured on CaP-coated pillar patterns with 10 ng/mL sRANKL or CaP-coated groove and hole patterns (height or depth, 10 μm) with 100 ng/mL sRANKL for 12 days. The cells were then removed from the surface of the pillars by immersing in 5% sodium hypochlorite for 3 min. The CaP-coated patterns were washed with water and dried, after which resorption pits on the patterns were observed by SEM after coating with Pt-Pd.

2.7 Animal experiments

First, patterned films with pillars (diameter and height, 1 and 5 μm or 5 and 5 μm) were treated with 120 s of plasma and cut into 2 × 4 mm pieces. An animal model of implantation was then established as previously described, with minor modifications [41]. Briefly, one male Wistar rat (7-week-old, approximately 200 g) was anesthetized, after which the pillar pattern was inserted into the medullary space through a 1 × 2 mm rectangular hole made in the femur (Fig. 1b). After 4 weeks of implantation, the rat was anaesthetized and perfused with 2.5% glutaraldehyde diluted in 0.1 M 4-(2-hydroxyethyl)-1-piperazineethanesulfonic acid buffer. The femur with the patterned film was extracted, fixed in 2.5% glutaraldehyde solution, and decalcified in 10% ethylenediaminetetraacetic acid. To prepare the sample for transmission electron microscopy

(TEM) [42], it was stained with 1% OsO_4, dehydrated, and embedded in Epon. This was followed by ultrathin sectioning and staining with uranyl acetate and lead citrate prior to TEM (JEM-1400, JEOL Ltd., Tokyo, Japan) at an acceleration voltage of 80 kV. Animal experiments were performed in accordance with the Guide for the Care and Use of Laboratory Animals and approved by Hokkaido University Committee (approval no. 20-0105).

2.8 Statistical analysis

Statistical analysis was performed using JMP Pro v14.0 (SAS Institute, Inc., Cary, NC, USA). All data are presented as the mean ± standard deviation (n = 6). Statistical differences were assessed by one-way analysis of variance with Tukey's multiple comparison post-hoc tests. p values < 0.05 were considered statistically significant.

3 Results

3.1 Morphology of multinucleated osteoclast-like cells on the patterned films

Overview of the experiments is shown as Fig. 1. To estimate cell attachment, the cells cultured on the patterns were observed via SEM. SEM images of multinucleated osteoclast-like cells derived from RAW264.7 cells on COP films after 6 days of culturing with RANKL are shown in Fig. 2. Small cells were RAW264.7 or mononucleated osteoclast-like cells. Numerous small, nondifferentiated RAW264.7 or small, mononuclear osteoclast-like cells were located around one multinucleated cell when under differentiation culture conditions. The patterned films were treated for 4 s with plasma because of the strong attachment of RAW264.7 cells to the surface of the substrates. We found that micro/nano-scale patterning of the COP planar surface affected the shape

and size of multinucleated osteoclast-like cells. Osteoclast-like cell areas on the planar, groove, and hole surfaces with a width or diameter of 500 nm, and a pillar with a diameter of 2 μm were smaller than those grown on pillars with diameters of 500 nm or 1 μm (Fig. 2a–f); indeed, the pillar shape markedly affected cell morphology (Fig. 2d–h). Osteoclast-like cells on pillars with diameters of 1 μm or 500 nm developed larger circular shapes than those on pillars with a diameter of 2 μm. Some of the filopodia appeared to grasp or cover the pillars. The cell periphery exhibited belt-like actin structure (Fig. 2e, f, and h). In contrast, cells on pillars with a diameter of 100 nm did not spread and seemed to weakly adhere to the patterned surface (Fig. 2g). The effect of the patterns on the osteoclast-like cell area was also supported by a quantitative analysis of cell area (Fig. S-1 in the ESM). The trend noted in the quantitative analysis of cell area on the patterns was similar to that observed in SEM images of the cell area. The following experiments will focus on the pillar pattern because characteristic morphologies of the cells on pillars were observed.

3.2 Osteoclast formation assay on the patterned films

We next investigated how the treatment time of plasma for COP surface wettability affects osteoclast formation from RAW264.7 cells. Fig. 3a shows the number of TRAP(+) multinucleated osteoclasts and contact angles of water on the planar and pillar (diameter and height, 500 and 500 nm) surfaces treated for 0, 1, 4, and 60 s with plasma. The contact angles gradually decreased from 94° to 38° for the planar surface and 114° to 17° for the pillar surface as plasma treatment time increased. The peak number of osteoclasts formed after 4 s of plasma treatment on both the planar and pillar surfaces. However, the total number of osteoclasts was 1.8-fold higher, on average, on the pillar pattern than on the planar surface ($p < 0.05$).

The effect of 4 s of plasma treatment on the different COP patterns, including grooves, holes, and pillars, on osteoclast formation was also determined (Fig. 3b). The peak number of osteoclasts

was observed for all patterns with a diameter or width of 500 nm, with the pillar pattern showing the highest number of osteoclasts. Patterns with a diameter or width of 2 μm had the lowest number of osteoclasts among all patterns with a height or depth of 500 nm. Interestingly, the pillar with a diameter of 100 nm had the lowest number of osteoclasts among all patterns.

Fig. 3c shows the results of multinucleation without RANKL and after 4 s of plasma treatment. The number of multinucleated cells was reduced to one-tenth the number of cells in the presence of RANKL. A small number of TRAP(+) multinucleated cells was observed for each pattern, and those with a diameter or width of 500 nm had the highest number of cells within their pattern group.

The number of TRAP(+) multinucleated osteoclasts on 4 s plasma-treated pillar patterns of different diameters and heights was also assessed (Fig. 3d). The number of osteoclasts on pillars with a diameter of 500 nm increased with increasing pillar height (500 nm to 2 μm), with the peak at 2 μm. In contrast, the number of osteoclasts on pillars with diameters of 1 μm or 2 μm was not influenced by increased pillar height. Comparison of the number of osteoclasts on the pillars with those on the grooves and holes of different widths or diameters and heights was also performed (Fig. S-2 in the EMS). The number of osteoclasts on pillars with a diameter of 500 nm apparently increased with increasing height, whereas the number of osteoclasts on grooves and holes did not show that trend.

We also investigated the effect of different pillar heights (500 nm to 2 μm; diameter, 500 nm; 4 s plasma) via immunofluorescence staining (Fig. 3f). Notably, the size and number of actin structures in osteoclasts were markedly influenced by increased pillar heights. Belt-like actin structures on the pillars were larger with increasing a height of pillar; the largest belt-like structure was observed on pillars with a diameter of 500 nm and a height of 2 μm. Moreover, osteoclast-like cells on the pillars with a height of 2 μm exhibited a greater number of nuclei and higher fusing activity than those on shorter pillars. On the planar surface, multinucleated osteoclast-like cells

were small (Fig. 3f, white arrows) and a belt-like actin structure was not observed under our culture conditions. Furthermore, the movement of osteoclast-like cells appeared hindered on pillars with a diameter of 10 μm, 5 μm, or 1 μm and a height of 10 μm (Fig. S-3a in the ESM) as compared with that on pillars with a height of 2 μm (Fig. 2h). The pillars with a diameter of 10 μm or 5 μm pushed up a part of cell body, transforming it into a cell with several attached pillars. The lamellipodia of the osteoclasts on pillars with a diameter of 1 μm invaded between pillars as shown in Fig. S-3a (iv) right image in the ESM. The formation of osteoclasts on pillars with a diameter of 1 μm was the highest among the 10 μm height pillar group (Fig. S-3b in the ESM).

Next, we monitored TRAP activity and belt-like structure formation in osteoclasts across the boundary between the planar and pillar (diameter and height, 500 nm and 2 μm; 4 s plasma treatment) surface after 6 days of culturing. Notably, strong TRAP staining of osteoclasts across the boundary was observed only on the pillar patterned side, with the planar side showing a weak staining intensity (Fig. 3g). Similar to TRAP activity, the semicircle belt-like structure showed a higher fluorescence intensity in osteoclasts on the pillar patterned side, compared with the faint intensity on the planar side (Fig. 3h).

3.3 Actin structure of multinucleated osteoclast-like cells on the pillar pattern

The actin structure of multinucleated osteoclast-like cells cultured from RAW264.7 cells on COP pillars (diameter, 1 or 5 μm; height, 2 or 10 μm) was evaluated using immunofluorescence (Fig. 4a and c). Actin structures appeared clearly on the pillar patterns; moreover, actin structures were influenced by the pillar diameter. On pillars with a diameter of 1 μm, the actin structure appeared as a large circle with a belt-like structure, whose diameter was on average 140 μm in the cell shown in Fig. 4a; interestingly, this large belt-like structure exhibited rows of small hollow circles (Fig. 4a, inset), which corresponded to a pillar diameter of 1 μm. Furthermore, the isolated

ring-like actin structures were mainly observed on pillars with a diameter of 5 μm and a height of 10 μm (Fig. 4c); Similarly, the isolated hollow circular shapes corresponded to a pillar diameter of 5 μm.

We next obtained a 3D reconstruction of multinucleated osteoclast-like cells cultured on COP pillars via CLSM (Fig. 4b and d). We found that the osteoclast-like cells were spread over a large number of pillars (Fig. 4b), and a large circle with a belt-like actin structure was observed at the cell periphery. Actin structure against the pillars consisted of small rings around the pillar base; rings that are fused or in contact with neighboring rings; and the rings wrapped over the pillars (Fig. 4b; i–iii). This first type formed on pillars with a diameter of 1 μm and a height of 2 μm as follows: (i) a small ring-like actin structure formed around and on the base of the pillars. The top view showed it as an isolated small hollow circle; (ii) the isolated ring-like structure developed further at the lower part of the pillars, and then neighboring isolated ring-like structures got in contact with each other or fused; (iii) the actin structure progressed upwards and became wrapped over the top of the pillar, which appeared as a filled circle from the top view (Fig. 4b; iii, top and side view).

In contrast, Fig. 4d shows multinucleated osteoclast-like cells spread over only a few pillars, with strongly or weakly appeared and isolated ring-like actin structures around the pillars with a diameter of 5 μm and a height of 10 μm. Interestingly, in the sectioned view, the 3D actin ring formed along the base and sides of the pillars (Fig. 4d; iv), whereas expression of actin filaments was faint at the top of the pillar.

The formation of a large belt-like and/or isolated ring actin structure changed according on pillar diameter (between 500 nm and 10 μm; Fig. S-4 in the ESM). However, it was difficult to develop

actin structures on pillars 100 nm or 50 μm in diameter and 200 nm or 10 μm in height or planar surfaces.

3.4 Pit formation assay on CaP-coated pillars

Next, we wondered whether resorption occurs in the actin structure space around a pillar, such as the sealing zone. To evaluate CaP resorption by osteoclasts, we performed a pit formation assay using CaP-coated pillars; the deposition of CaP nanoparticles covered most of the pillar surface (Fig. S-5c in the ESM). After performing the assay, the smooth surface of the COP pillars indicated that the CaP coating was completely resorbed, as evidenced by SEM (Fig. 4e). Moreover, CaP resorption pits were observed on the convex part of the isolated pillar but not on the planar floor (Fig. 4e; middle panel). SEM images acquired at a 45° tilt angle showed that resorption of the CaP coating was completed at the top of the pillars but was comparatively in progress near pillar base, resulting a decreased roughness of the CaP coating surface (Fig. 4e; bottom panel).

3.5 Actin structure and pit formation assay on groove and hole patterns

We also evaluated the actin structure and pit formation on groove and hole patterned surfaces with a width or diameter of 5 μm and a depth of 10 μm (Fig. 5). However, the cells were differentiated at a high concentration (100 ng/mL) of sRANKL because it is harder for the cells to develop actin structures on groove and hole patterns than on pillar patterns. Fig. 5a shows that actin structures on the ridge formed along the long axis of the groove/ridge pattern direction, forming a rectangular shape. Pit formation on the CaP-coated groove pattern demonstrated a rectangular resorption pit on the ridge of the groove/ridge pattern (Fig. 5b). For the hole pattern, small dots appeared inside holes, corresponding to the hole diameter, within a large belt-like actin structure corresponding to the cell periphery (Fig. 5c). Pit formation on the CaP-coated holes

showed resorption pits at the planar surface of the hole pattern (Fig. 5d). Notably, there were two different types of resorption modes inside the hole within the resorption pit: resorption inside hole and non-resorption inside hole (Fig. 5d; illustrations).

It is noteworthy that osteoclasts can change actin structures according to the pattern size, shape, and height (Fig. S-4 in the ESM). Furthermore, a wide variety of actin structures on the high aspect patterns was observed at a high concentration of sRANKL (100 ng/mL) (Fig. S-6 in the ESM). Large belt-like actin structures and/or the fusion structures of rings or half circle rings were observed on pillars and holes.

3.6 Animal implantation model

Lastly, we focused our attention to the sealing zones formed by osteoclasts against the pillars *in vivo*. To assess the pillar pattern performance *in vivo*, COP pillars (diameter and height, 1 and 5 μm, or 5 and 5 μm; 120 s plasma treatment) were implanted into a rat femur for 4 weeks; Fig. 4f shows the TEM images of the decalcified specimen between the bone matrix and pillars. Osteoclast-like cells were found to be in contact with the pillar surface. The pillars appeared to be pushing against the cells and sinking the cell body. Furthermore, on the pillars (diameter and height, 1 and 5 μm), some pillars were covered with sealing zones formed by the osteoclast-like cells; some sealing zones formed as isolated pillars covers that were in contact with each other (Fig. 4f; A), whereas other sealing zones were fused at the base of the pillars (Fig. 4f; B). The pillars (diameter and height, 5 and 5 μm) showed some sealing zones formed at their base and sides (Fig. 4f; C), indicating an isolated, ring-like actin structure at the base of the pillars.

4 Discussion

4.1 Effect of pattern size and shape on osteoclast formation

In the present study, we investigated systematic patterns with defined shapes with a 1:1 pitch ratio to reveal the optimum structural factors, such as 2D size, height, and shape, for osteoclast formation and function.

Regarding the 2D size factor, submicron-sized patterns, but not micron- and nano-sized patterns, strongly induced osteoclast formation. Thus, patterns with a diameter or width of 500 nm appear suitable for pre-osteoclast adhesion and induce osteoclast formation. Previously, we reported that the number of attached RAW264.7 cells are higher on pillars with a diameter of 500 nm than a diameter of 2 μm [33]; however, this reduced cell adhesion was not linked to the development of actin structure as an adhesion apparatus. We thus speculated that the pattern itself directly stimulates pre-osteoclasts or osteoclasts to induce osteoclast formation or function. This may occur via mechanotransduction, where osteoclasts translate mechanical cues from the substrate's texture into chemical signals via actin structures such as podosomes [43, 44]. Our observations of osteoclasts across the pillar and planar surface borders indicate that the cells are directly stimulated by the pillar structure, promoting TRAP activity and belt-like actin pattern formation (Fig. 3g and h). It is possible that submicron-sized patterns (e.g., 500 nm in diameter) effectively stimulate pre-osteoclasts owing to the presence of many pillars of optimal size that directly stimulate the cell. In contrast, nano-sized pillars (100 nm in diameter) reduced osteoclast formation as it was difficult for pre-osteoclast RAW264.7 cells to adhere and spread well (Fig. 2g), and thus they were unable to differentiate and fuse (Fig. 3b).

Regarding pattern height, pillars (diameter, 500 nm) with a height of 2 μm were optimum for osteoclast formation (Fig. 3d, f, and S-2). Taking our findings into consideration, it can be

concluded that the optimal pattern dimensions promote cell adhesion, influence cell motility, and stimulate pre-osteoclasts, thereby promoting osteoclast formation. Indeed, cells on tall pillars (10 μm) had difficulty moving over them as the height became an obstruction (Fig. S-3 in the ESM). It is thus necessary to balance stimulation and obstruction by optimizing the size and height of the patterns.

In terms of shape, osteoclast formation was induced in the order pillar > groove ≥ hole. One explanation is that osteoclast formation is influenced by the upper surface area or convex volume of the pattern shapes. As mentioned previously, sealing zone rings preferentially develop around protrusion of bone slices with lateral dimensions of several micrometers and ~1 μm in height [9]. This preferential interaction of osteoclasts with protrusions is similar to our results showing preferential osteoclast formation on pillars. Another possibility is that osteoclasts are highly activated by patterns with a high-density of small stimulating shapes, such as submicron-sized pillars.

Other than structural factors, surface wettability can also affect osteoclast formation and function [13, 45–47]. However, the relationship between wettability and osteoclastogenesis is unclear, and previous studies employed non-uniform topographic substrates without altering wettability. By testing different wettability conditions, we demonstrated that RAW264.7 cells prefer hydrophilic surfaces for osteoclast formation. Moreover, a 30° contact angle for pillars (diameter and height, 500 and 500 nm) and a 46° contact angle for the planar surface exhibited the highest osteoclast numbers. The contact angles at a peak for osteoclast formation were estimated under limited interval times (0, 1, 4, and 60 s) of plasma treatment so its value could be roughly estimated. At least, there is a nonlinear relationship between wettability and osteoclast formation, indicating that both wettability and topography of the patterns should be optimized.

The optimal topography for osteoclast formation and function has not been fully determined using rough-surfaced substrates. In grain-fused beta-tricalcium phosphate disks, the submicron-scale surface (R_a = 0.13 μm) promotes higher TRAP activity compared with the micron-scale surface (R_a = 1.29 μm) [11]. In contrast, on a sandblasted titanium surface, the number of osteoclasts increases with increasing roughness (R_a = 0.24–3.63 μm) [14]. Although these studies demonstrate that osteoclast formation and activity are affected by surface roughness [12, 13], the correlation appears nonlinear. In many cases, submicron-scale surfaces induce osteoclast formation and function, whereas nano- and micron-scale surfaces are not as effective. In other cases, this trend is not observed. These incongruent results may have resulted from the substrates having structural irregularities.

Osteoclast function and formation have not been examined in detail on defined patterns (e.g., pillar, hole, groove) at the micron or nano level, owing to the limited variations in pattern structural patterns [17–23]. One study reported that these patterns induce osteoclast formation and function, where osteoclastogenic differentiation of RAW264.7 cells was promoted on bioactive glass microgrooves with a ridge width of 10 μm, groove width of 30 μm, and groove depth of 8 μm [17]. In contrast, these patterns were found to reduce osteoclastogenesis, as osteoclastogenic differentiation was significantly inhibited in RAW264.7 cells on PLC disks with concentric circular microgrooves 20 μm in width and 20 μm in height compared with parallel linear microgrooves and flat surfaces [19]. No previous studies have used the exact same sized patterns as ours (optimal size: pillar with a diameter of 500 nm and height 2 μm). However, our optimized pattern is supported by other reported similar surfaces/materials that promote the development of osteoclast-like cells *in vitro* and/or *in vivo*, such as grain-fused beta-tricalcium phosphate disks with grain size of approximately 1 μm [11, 48], porous HA disks with graine size of approximately 500 nm [13], and plate-like octacalcium phosphate crystals with a width within 0.3 to 2.0 μm [49].

Nonetheless, the optimal pattern size may slightly change depending on the cell type or the conditions being investigated. These findings indicate that osteoclast formation and function is dependent on the size and shape of the defined patterns. Indeed, our findings revealed that osteoclastogenesis can be controlled by varying the pattern size and shape.

4.2 Actin structure and resorption pit formation on the patterned surfaces

F-actin structure in osteoclasts contributes to cell adhesion, mechanotransduction, and bone resorption [44, 50, 51]. Immature or mature osteoclasts control the aggregation, shape, and movement of actin filaments during osteoclast differentiation. The cells form distinctive actin patterns, such as actin rings or clusters, podosome belts, and sealing zones. Moreover, the formation and shape of these actin patterns are influenced by substrate type and roughness [9, 52, 53].

In this study, highly expressed actin filaments and characteristic actin structure were identified on and around pillars (Fig. 4). Notably, actin structure exhibited different shapes depending on the size and height of the pillars. We observed two types of actin structure, and both displayed hollow circles. The first type consisted of a large belt-like actin structure with small hollow circles (Fig. 4a and b) that formed on pillars with a diameter of 1 μm and a height of 2 μm and the second type was an isolated, ring-like actin structure around pillars with a diameter of 5 μm and a height of 10 μm. The first type was also observed wrapped around the implanted pillars (diameter and height, 1 and 5 μm) of the rat femoral implant model. The second type was also observed in an actin structure at sides of pillars (diameter and height, 5 and 5 μm) *in vivo*, the actin structure can be presumed to be an isolated, ring-like actin structure around the implanted pillars. These *in vivo* observations indicate that primary osteoclasts also form unique actin structures against pillars *in*

vivo. Furthermore, a wide variety of actin structures appeared by controlling pattern structural factors and RANKL concentration (Fig. 5, S-4 and S-6 in the ESM).

One advantage of using defined patterns is the ease of observing how the actin structure adapts to different patterns [53]. Using fluorescence microscopy, we demonstrated a clear adaptation of actin structure to the pillar shape. Generally, it is difficult to judge the adaptation of actin to rough surfaces owing to the irregular structural factors of the substrates. Nevertheless, previous studies have shown that the size and shape of actin structures in osteoclasts change according to certain factors, such as substrate roughness and composition. Geblinger et al. [52] reported that translocation of the sealing zone is arrested by the sharp edges of topographical obstacles on sandblasted rough surfaces. Thus, studies indicate that actin structure, such as the sealing zone [9], can adapt to patterns based on their specific structural properties.

Osteoclast resorptive activity is largely influenced by surface roughness and porosity [4, 11–13, 15, 16, 54]. Previous studies have indicated that sufficient substrate roughness is necessary for high resorption activity. However, it has not been clarified whether resorption pit formation responds to the substrate surface shape. Here, we showed that osteoclasts preferentially exhibit resorption on convex shapes such as pillars, given the higher number of osteoclasts on pillars than on holes; the formation of ring-like actin structures at the base of the pillars, which was especially remarkable on the 5 μm pillar; and resorption occurring at the top of the pillar, not at the flat bottom surface except a convex part of pillar pattern. Furthermore, resorption occurred at the top of the groove and hole surfaces. Höner et al. [17] reported that resorption pits are observed in the grooves and on the groove walls of a bioactive glass groove [17]; this disagrees with our results, in which resorption pits formed at top part of the groove/ridge patterns (Fig. 5b). This discrepancy may have resulted from the bioactive glass groove having a smooth instead of a sharp edge, and thus the

osteoclasts could not recognize it. Therefore, it is possible that patterns with sharp edges are important for triggering the osteoclast resorption response.

Osteoclasts may sense surface topography, and osteoclast precursors may possess specific sensors that detect rough surfaces to initiate differentiation into mature osteoclasts [16]. Relationships between osteoclastic activity and bone surface roughness or imperfections *in vivo* have been suggested by previous studies [8, 9, 16]; for instance, it is conceivable that old and damaged bone is considerably rougher than newly formed bone [8]. Overall, our study also supports the notion that bone resorption is mediated by surface topography sensing of osteoclasts.

There are some limitations associated with our study. We used the mouse macrophage cell line RAW264.7, which is a model osteoclast precursor; however, to further investigate the effect of different patterns on osteoclasts, primary pre-osteoclasts or primary monocyte/macrophage hematopoietic lineage cells should also be employed. Moreover, the variations in the tested systematic patterns were still limited, i.e. further higher patterns or patterns with varying chemical composition. The effect of wettability for osteoclastogenesis was investigated within preset contact angles so this approach could show a rough indication of the peak of osteoclastogenesis. One of the important factors of patterns is known as pitch, which in the present study were all designed as a 1:1 pitch ratio. Further studies are warranted to explore in greater detail the impact of the pitch factor in patterns on osteoclastogenesis so to elucidate the underlying mechanism for osteoclastogenesis induction.

5 Conclusions

In summary, we prepared systematic micro/nano-scale patterns with a 1:1 pitch and evaluated their effect on osteoclastogenesis. The optimal structural factors for osteoclast formation and function from pre-osteoclastic RAW264.7 cells were submicron-sized pillar patterns with a diameter of 500 nm and a height of 2 μm. We also identified two types of characteristic actin structures on and around pillars depending on the pillar dimensions as well as resorption of CaP-coated pillars that mainly occurred at the top of the pillars. This indicates that osteoclasts prefer convex shapes for the formation of resorption pits. Notably, osteoclasts can change their resorption style by adapting their actin structures to different pattern sizes and shapes. Taken together, these results indicate that osteoclast formation from RAW264.7 cells can be highly promoted by limited morphological shapes, and that precise surface design is pivotal for controlling pre-osteoclast and osteoclast function. These findings can aid the design of bone prosthetic and replacement material surfaces.

Our study also supports the notion that osteoclasts may sense surface topography as a mechanism of bone resorption. Moreover, defined patterns will help elucidate several unclear mechanisms underlying osteoclast formation, function, and resorption. The questions that need to be addressed in future studies are as follows: Is the effect of pattern compositions, e.g., apatite and collagen pattern, on osteoclastogenesis? Can osteoclasts resorb on how height of pattern? How do osteoclasts recognize the height of pattern in molecular biology? Which pattern is best for osteoclastogenesis *in vivo*?

Acknowledgements

This work was supported by JSPS KAKENHI [grant numbers JP25463047, JP18K18984, JP19H03839, JP19H04461]. We are grateful to the support provided by the Central Research

Institute of Hokkaido University and the Electron Microscope Laboratory at the Research Faculty of Agriculture of Hokkaido University, where fluorescence and confocal microscopy was performed, respectively. We would also like to thank the Nanotechnology Platform Japan H25 FS program “A trial use of the nanotechnology research facility” (F-13-HK-0055) for providing silicon molds with 100 nm deep holes. We would like to thank Editage (www.editage.jp) for English language editing.

Electronic Supplementary Material: Supplementary material (area of osteoclast-like cells, effect of height or depth of the patterns on osteoclastogenesis, effect of tall pillar on osteoclast formation, immunofluorescence images of actin structures on different COP patterns, SEM images of CaP-coated patterns, and immunofluorescence images of actin structures on the high aspect patterns at a high concentration of sRANKL) is available in the online version of this article at http://dx.doi.org/10.1007/ **********.

References

[1] Marchisio, M.; Di Carmine, M.; Pagone, R.; Piattelli, A.; Miscia, S. Implant surface roughness influences osteoclast proliferation and differentiation. *J. Biomed. Mater. Res. B Appl. Biomater.* **2005**, *75*, 251–256.

[2] Boyce, B. F.; Yao, Z.; Xing, L. Osteoclasts have multiple roles in bone in addition to bone resorption. *Crit. Rev. Eukaryot. Gene Expr.* **2009**, *19*, 171–180.

[3] Novack, D. V.; Teitelbaum, S. L. The osteoclast: friend or foe? *Annu. Rev. Pathol.* **2008**, *3*, 457–484.

[4] Webster, T. J.; Ergun, C.; Doremus, R. H.; Siegel, R. W.; Bizios, R. Enhanced osteoclast-like cell functions on nanophase ceramics. *Biomaterials* **2001**, *22*, 1327–1333.

[5] Nguyen, J.; Nohe, A. Factors that affect the osteoclastogenesis of RAW264.7 cells. *J. Biochem. Anal. Stud.* **2017**, *2*.

[6] Detsch, R.; Boccaccini, A. R. The role of osteoclasts in bone tissue engineering. *J. Tissue Eng. Regen. Med.* **2015**, *9*, 1133–1149.

[7] Boyan, B. D.; Lotz, E. M.; Schwartz, Z. Roughness and hydrophilicity as osteogenic biomimetic surface properties. *Tissue Eng. Part A* **2017**, *23*, 1479–1489.

[8] Geblinger, D.; Addadi, L.; Geiger, B. Nano-topography sensing by osteoclasts. *J. Cell Sci.* **2010**, *123*, 1503–1510.

[9] Shemesh, M.; Addadi, S.; Milstein, Y.; Geiger, B.; Addadi, L. Study of osteoclast adhesion to cortical bone surfaces: a correlative microscopy approach for concomitant imaging of cellular dynamics and surface modifications. *A.C.S. Appl. Mater. Interfaces* **2016**, *8*, 14932–14943.

[10] Ciapetti, G.; Di Pompo, G.; Avnet, S.; Martini, D.; Diez-Escudero, A.; Montufar, E. B.; Ginebra, M. P.; Baldini, N. Osteoclast differentiation from human blood precursors on biomimetic calcium–phosphate substrates. *Acta Biomater.* **2017**, *50*, 102–113.

[11] Davison, N. L.; ten Harkel, B.; Schoenmaker, T.; Luo, X.; Yuan, H.; Everts, V.; Barrère-de Groot, F.; de Bruijn, J. D. Osteoclast resorption of beta-tricalcium phosphate controlled by surface architecture. *Biomaterials* **2014**, *35*, 7441–7451.

[12] Costa, D. O.; Prowse, P. D.; Chrones, T.; Sims, S. M.; Hamilton, D. W.; Rizkalla, A. S.; Dixon, S. J. The differential regulation of osteoblast and osteoclast activity by surface topography of hydroxyapatite coatings. *Biomaterials* **2013**, *34*, 7215–7226.

[13] Chen, F.; Wang, M.; Wang, J.; Chen, X.; Li, X.; Xiao, Y.; Zhang, X. Effects of hydroxyapatite surface nano/micro-structure on osteoclast formation and activity. *J. Mater. Chem. B* **2019**, *7*, 7574–7587.

[14] Zhang, Y.; Chen, S. E.; Shao, J.; van den Beucken, J. J. J. P. Combinatorial surface roughness effects on osteoclastogenesis and osteogenesis. *A.C.S. Appl. Mater. Interfaces* **2018**, *10*, 36652–36663.

[15] Matsunaga, T.; Inoue, H.; Kojo, T.; Hatano, K.; Tsujisawa, T.; Uchiyama, C.; Uchida, Y. Disaggregated osteoclasts increase in resorption activity in response to roughness of bone surface. *J. Biomed. Mater. Res.* **1999**, *48*, 417–423.

[16] Costa-Rodrigues, J.; Fernandes, A.; Lopes, M. A.; Fernandes, M. H. Hydroxyapatite surface roughness: complex modulation of the osteoclastogenesis of human precursor cells. *Acta Biomater.* **2012**, *8*, 1137–1145.

[17] Höner, M.; Lauria, I.; Dabhi, C.; Kant, S.; Leube, R. E.; Fischer, H. Periodic microstructures on bioactive glass surfaces enhance osteogenic differentiation of human mesenchymal stromal cells and promote osteoclastogenesis in vitro. *J. Biomed. Mater. Res. A* **2018**, *106*, 1965–1978.

[18] Takata, R.; Akasaka, T.; Tamai, M.; Yoshimura, Y.; Taira, T.; Miyaji, H.; Tagawa, Y.; Yamagata, S.; Iida, J.; Yoshida, Y. Effect of a nano-scale fine hole pattern on the differentiation of RAW264.7 cells into osteoclasts. *Dig., J. Nanomater. Biostruct* **2018**, *13*, 451–458.

[19] Li, M.; Fu, X.; Gao, H.; Ji, Y.; Li, J.; Wang, Y. Regulation of an osteon-like concentric microgrooved surface on osteogenesis and osteoclastogenesis. *Biomaterials* **2019**, *216*, 119269.

[20] Silverwood, R. K.; Fairhurst, P. G.; Sjöström T.; Welsh, F.; Sun, Y.; Li, G.; Yu, B.; Young, P. S.; Su, B.; Meek, R. M. et al. Analysis of osteoclastogenesis/osteoblastogenesis on nanotopographical titania surfaces. *Adv. Healthc. Mater.* **2016**, *5*, 947–955.

[21] Halai, M.; Ker, A.; Meek, R. D.; Nadeem, D.; Sjostrom, T.; Su, B.; McNamara, L. E.; Dalby, M. J.; Young, P. S. Scanning electron microscopical observation of an osteoblast/osteoclast co-culture on micropatterned orthopaedic ceramics. *J. Tissue Eng.* **2014**, *5*, 2041731414552114.

[22] Young, P. S.; Tsimbouri, P. M.; Gadegaard, N.; Meek, R. M.; Dalby, M. J. Osteoclastogenesis/osteoblastogenesis using human bone marrow-derived cocultures on nanotopographical polymer surfaces. *Nanomedicine (Lond)* **2015**, *10*, 949–957.

[23] Niida, A.; Abiko, Y.; Yui, T.; Hirose, Y.; Ochi, M. Effect of surface topography on osteoclast-like cell behavior. *J. Jpn. Soc. Oral Implantol.* **2013**, *26*, 651–659 (in Japanese).

[24] Chou, S. Y.; Krauss, P. R.; Renstrom, P. J. Nanoimprint lithography. *J. Vac. Sci. Technol. B* **1996**, *14*, 4129–4133.

[25] van Dommelen, R.; Fanzio, P.; Sasso, L. Surface self-assembly of colloidal crystals for micro- and nano-patterning. *Adv. Colloid Interface Sci.* **2018**, *251*, 97–114.

[26] Mishra, S.; Yadava, V. Laser beam micromachining (LBMM) – a review. *Opt. Lasers Eng.* **2015**, *73*, 89–122.

[27] Lima, M. J.; Correlo, V. M.; Reis, R. L. Micro/nano replication and 3D assembling techniques for scaffold fabrication. *Mater. Sci. Eng. C Mater. Biol. Appl.* **2014**, *42*, 615–621.

[28] Anselme, K.; Davidson, P.; Popa, A. M.; Giazzon, M.; Liley, M.; Ploux, L. The interaction of cells and bacteria with surfaces structured at the nanometre scale. *Acta Biomater.* **2010**, *6*, 3824–3846.

[29] Dobbenga, S.; Fratila-Apachitei, L. E.; Zadpoor, A. A. Nanopattern-induced osteogenic differentiation of stem cells – a systematic review. *Acta Biomater.* **2016**, *46*, 3–14.

[30] Jaggessar, A.; Shahali, H.; Mathew, A.; Yarlagadda, P. K. D. V. Bio-mimicking Nano and micro-structured surface fabrication for antibacterial properties in medical implants. *J. Nanobiotechnology* **2017**, *15*, 64.

[31] Dai, J.; Yao, Y. Adaptive ordering and filament polymerization of cell cytoskeleton by tunable nanoarrays. *Nano Res.* **2021**, *14*, 620–627.

[32] Lorite, G. S.; Ylä-Outinen, L.; Janssen, L.; Pitkänen, O.; Joki, T.; Koivisto, J. T.; Kellomäki, M.; Vajtai, R.; Narkilahti, S.; Kordas, K. Carbon nanotube micropillars trigger guided growth of complex human neural stem cells networks. *Nano Res.* **2019**, *12*, 2894–2899.

[33] Honma, J.; Akasaka, T.; Tamai, M.; Yoshimura, Y.; Taira, T.; Miyaji, H.; Yamagata, S.; Sato, Y.; Yoshida, Y. Fusion of RAW 264.7 macrophage cells on micro scale fine pillar patterns. *Dig., J. Nanomater. Biostruct* **2018**, *13*, 1123–1131.

[34] Yamazaki, M. Industrialization and application development of cyclo-olefin polymer. *J. Mol. Catal. A: Chemical* **2004**, *213*, 81–87.

[35] Strehmel, C.; Perez-Hernandez, H.; Zhang, Z.; Löbus, A.; Lasagni, A. F.; Lensen, M. C. Geometric control of cell alignment and spreading within the confinement of antiadhesive poly(ethylene glycol) microstructures on laser-patterned surfaces. *A.C.S. Biomater. Sci. Eng.* **2015**, *1*, 747–752.

[36] Akasaka, T.; Yokoyama, A.; Matsuoka, M.; Hashimoto, T.; Watari, F. Thin films of single-walled carbon nanotubes promote human osteoblastic cells (Saos-2) proliferation in low serum concentrations. *Mater. Sci. Eng. C* **2010**, *30*, 391–399.

[37] Omori, A.; Yoshimura, Y.; Deyama, Y.; Suzuki, K. Rosmarinic acid and arbutin suppress osteoclast differentiation by inhibiting superoxide and NFATc1 downregulation in RAW 264.7 cells. *Biomed. Rep.* **2015**, *3*, 483–490.

[38] Miyazaki, T.; Miyauchi, S.; Anada, T.; Imaizumi, H.; Suzuki, O. Evaluation of osteoclastic resorption activity using calcium phosphate coating combined with labeled polyanion. *Anal. Biochem.* **2011**, *410*, 7–12.

[39] Maria, S. M.; Prukner, C.; Sheikh, Z.; Mueller, F.; Barralet, J. E.; Komarova, S. V. Reproducible quantification of osteoclastic activity: characterization of a biomimetic calcium phosphate assay. *J. Biomed. Mater. Res. B Appl. Biomater.* **2014**, *102*, 903–912.

[40] Wen, H. B.; De Wijn, J. R.; Liu, Q.; De Groot, K.; Cui, F. Z. A simple method to prepare calcium phosphate coatings on Ti6Al4V. *J. Mater. Sci. Mater. Med.* **1997**, *8*, 765–770.

[41] Takada, S.; Hirata, E.; Sakairi, M.; Miyako, E.; Takano, Y.; Ushijima, N.; Yudasaka, M.; Iijima, S.; Yokoyama, A. Carbon nanohorn coating by electrodeposition accelerate bone formation on titanium implant. *Artif. Cells Nanomed. Biotechnol.* **2021**, *49*, 20–29.

[42] Shitomi, K.; Miyaji, H.; Miyata, S.; Sugaya, T.; Ushijima, N.; Akasaka, T.; Kawasaki, H. Photodynamic inactivation of oral bacteria with silver nanoclusters/rose bengal nanocomposite. *Photodiagnosis Photodyn. Ther.* **2020**, *30*, 101647.

[43] van den Dries, K.; Bolomini-Vittori, M.; Cambi, A. Spatiotemporal organization and mechanosensory function of podosomes. *Cell Adh. Migr.* **2014**, *8*, 268–272.

[44] Linder, S.; Wiesner, C. Feel the force: Podosomes in mechanosensing. *Exp. Cell Res.* **2016**, *343*, 67–72.

[45] More, S. E.; Dave, J. R.; Makar, P. K.; Bhoraskar, S. V.; Premkumar, S.; Tomar, G. B.; Mathe, V. L. Surface modification of UHMWPE using ECR plasma for osteoblast and osteoclast differentiation. *Appl. Surf. Sci.* **2020**, *506*, 144665.

[46] Costa-Rodrigues, J.; Carmo, S.; Perpétuo, I. P.; Monteiro, F. J.; Fernandes, M. H. Osteoclastogenic differentiation of human precursor cells over micro- and nanostructured hydroxyapatite topography. *Biochim. Biophys. Acta* **2016**, *1860*, 825–835.

[47] Redey, S. A.; Razzouk, S.; Rey, C.; Bernache-Assollant, D.; Leroy, G.; Nardin, M. Cournot, G. Osteoclast adhesion and activity on synthetic hydroxyapatite, carbonated hydroxyapatite, and natural calcium carbonate: relationship to surface energies. *J. Biomed. Mater. Res.* **1999**, *45*, 140–147.

[48] Davison, N. L.; Su, J.; Yuan, H.; van den Beucken, J. J. J. P.; de Brujin, J. D; Barrère-de Groot, F. Influence of surface microstructure and chemistry on osteoinduction and osteoclastogenesis by biphasic calcium phosphate discs. *Eur. Cell. Mater.* **2015**, *29*, 314–329.

[49] Shiwaku, Y.; Hamai, R.; Sato, S.; Sakai, S.; Tsuchiya, K.; Baba, K.; Takahashi, T.; Suzuki, O. Bone tissue response to different grown crystal batches of octacalcium phosphate in rat long bone intramedullary canal area. *Int. J. Mol. Sci.* **2021**, *22*, 9770.

[50] Schachtner, H.; Calaminus, S. D.; Thomas, S. G.; Machesky, L. M. Podosomes in adhesion, migration, mechanosensing and matrix remodeling. *Cytoskeleton (Hoboken)* **2013**, *70*, 572–589.

[51] Saltel, F.; Chabadel, A.; Bonnelye, E.; Jurdic, P. Actin cytoskeletal organisation in osteoclasts: a model to decipher transmigration and matrix degradation. *Eur. J. Cell Biol.* **2008**, *87*, 459–468.

[52] Geblinger, D.; Zink, C.; Spencer, N. D.; Addadi, L.; Geiger, B. Effects of surface microtopography on the assembly of the osteoclast resorption apparatus. *J. R. Soc. Interface* **2012**, *9*, 1599–1608.

[53] Anderegg, F.; Geblinger, D.; Horvath, P.; Charnley, M.; Textor, M.; Addadi, L.; Geiger, B. Substrate adhesion regulates sealing zone architecture and dynamics in cultured osteoclasts. *PLOS ONE* **2011**, *6*, e28583.

[54] Gross, K. A.; Muller, D.; Lucas, H.; Haynes, D. R. Osteoclast resorption of thermal spray hydoxyapatite coatings is influenced by surface topography. *Acta Biomater.* **2012**, *8*, 1948–1956.

Figure captions

Figure 1 Diagrams illustrating the (a) osteoclast formation assay and (b) actin structure or pit formation on cyclo-olefin polymer (COP) micro/nano-scale patterns *in vitro* or *in vivo*.

Figure 2 SEM images at a 45° tilt angle of multinucleated osteoclast-like cells derived from RAW264.7 cells on COP micro/nano-scale patterns after 6 days of culturing with RANKL. The surface patterns were treated with plasma for 4 s. (a–h) Representative images of cells on different patterns with varying diameters, width, height or depth. The dotted squares on the left panels are magnified in the corresponding right panels. Scale bar = 2 μm. White arrows indicate multinucleated osteoclast-like cells. Small cells are RAW264.7 or mononucleated osteoclast-like cells. Dimensions are indicated as pattern diameter (φ), width (w)/height (h), or depth (d).

Figure 3 Osteoclast formation assay of RAW264.7 cells on COP micro/nano-scale patterns after 6 days of culturing with or without RANKL. (a) Number of multinucleated cells on the planar surface and pillars in the presence of RANKL. The numbers at the top indicate the contact angle (°). (b) Number of multinucleated cells on groove, hole, and pillar patterns after 4 s of plasma treatment in the presence of RANKL. (c) Multinucleated cell number without RANKL. (d) The effect of pillar height on cell number. TCPS, tissue culture polystyrene. Significant differences between groups are indicated above each column with different lowercase letters ($p < 0.05$). (f) Representative immunofluorescence images of cells on the planar surface and pillars. Dimensions are indicated as pillar diameter (φ)/height (h). Red, F-actin; blue, nuclei. White arrows indicate multinucleated osteoclast-like cells on the planar substrate. (g) Bright field image of TRAP-stained multinucleated osteoclasts across the boundary between the planar surface and pillar. (h) Left panel,

immunofluorescence of multinucleated osteoclast-like cells across the boundary between the planar surface and pillar. Red, F-actin; green, vinculin; blue, nuclei. Right panel, illustration of the belt-like actin structure observed across the boundary.

Figure 4 2D immunofluorescence (a and c) and orthogonal section views (b and d) of multinucleated osteoclast-like cells from RAW264.7 cells on COP pillars. The cells were cultured on 4 s of plasma-treated pillars with RANKL for 6 days. Dimensions are indicated as pillar diameter (φ)/height (h). Red, F-actin; green, vinculin; blue, nuclei. The fluorescence images and one bright field image were merged. Orthogonal section views were obtained, and then 3D images were reconstructed by confocal laser scanning microscopy (CLSM). i–iv regions in the cross-sectional side views (b, d) correspond to the i–iv illustrations below the panels to visualize the type of actin structure observed. (e) Pit formation assay. Top panel: diagram showing the preparation of a calcium phosphate (CaP)-coated pillar. Middle and bottom panels: scanning electron microscopy (SEM) of CaP-coated pillars showing the top view (middle) and at a 45° tilt angle (bottom). White arrows indicate complete resorption of CaP coating by osteoclasts. Black arrows indicate in progress resorption of CaP coating. (f) Animal implantation model. The COP films with pillar patterns (diameter/height) were implanted in a rat femur for 4 weeks. Transmission electron microscopy (TEM) showing osteoclast contact with pillars. An osteoclast sealing zone (SZ) covered on the pillars, or which some were formed at the base and sides of the pillars. Right images show a magnified view. Illustrations demonstrate how the SZ formed around the pillars.

Figure 5 Immunofluorescence and pit formation assay of groove and hole patterns. Dimensions are indicated as pattern diameter (φ) or width (w)/depth (d). (a, c) The cells were cultured on 4 s plasma-treated patterns in the presence of 100 ng/mL sRANKL for 6 days. Red, F-actin; green, vinculin; blue, nuclei. Three fluorescence images and one bright field image were merged. (b, d) Pit formation assay on CaP-coated patterns. SEM images were acquired at a 45° tilt angle. Illustrations on the right demonstrate the different resorption styles of osteoclasts on the hole pattern.

Figures

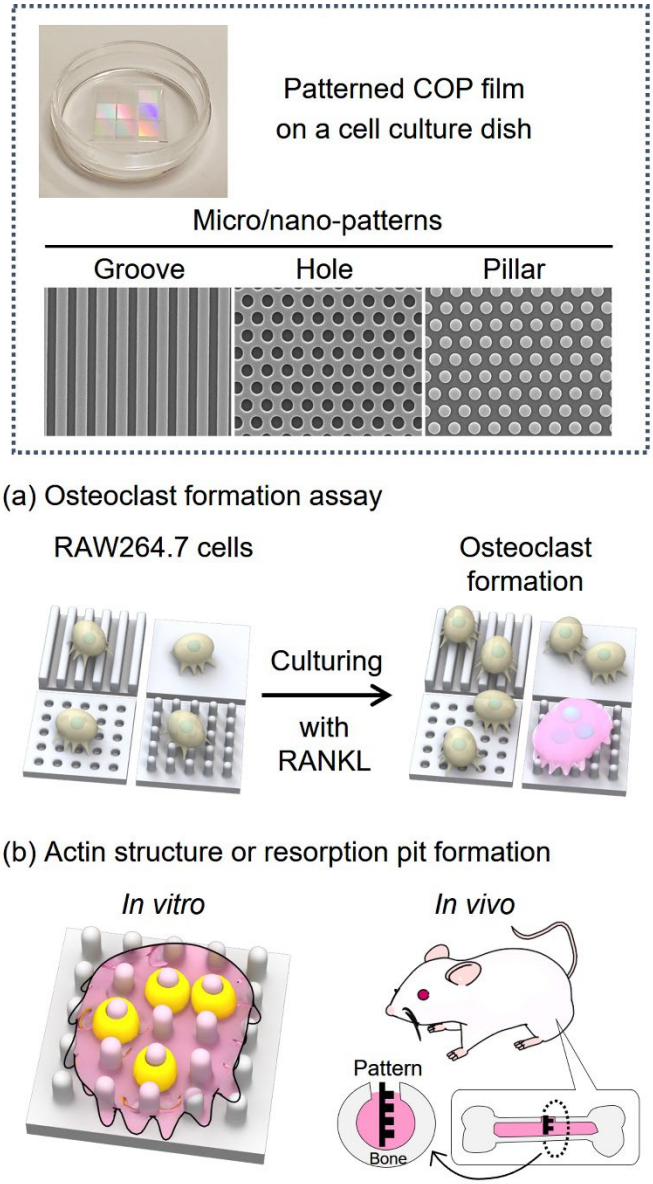

Figure 1

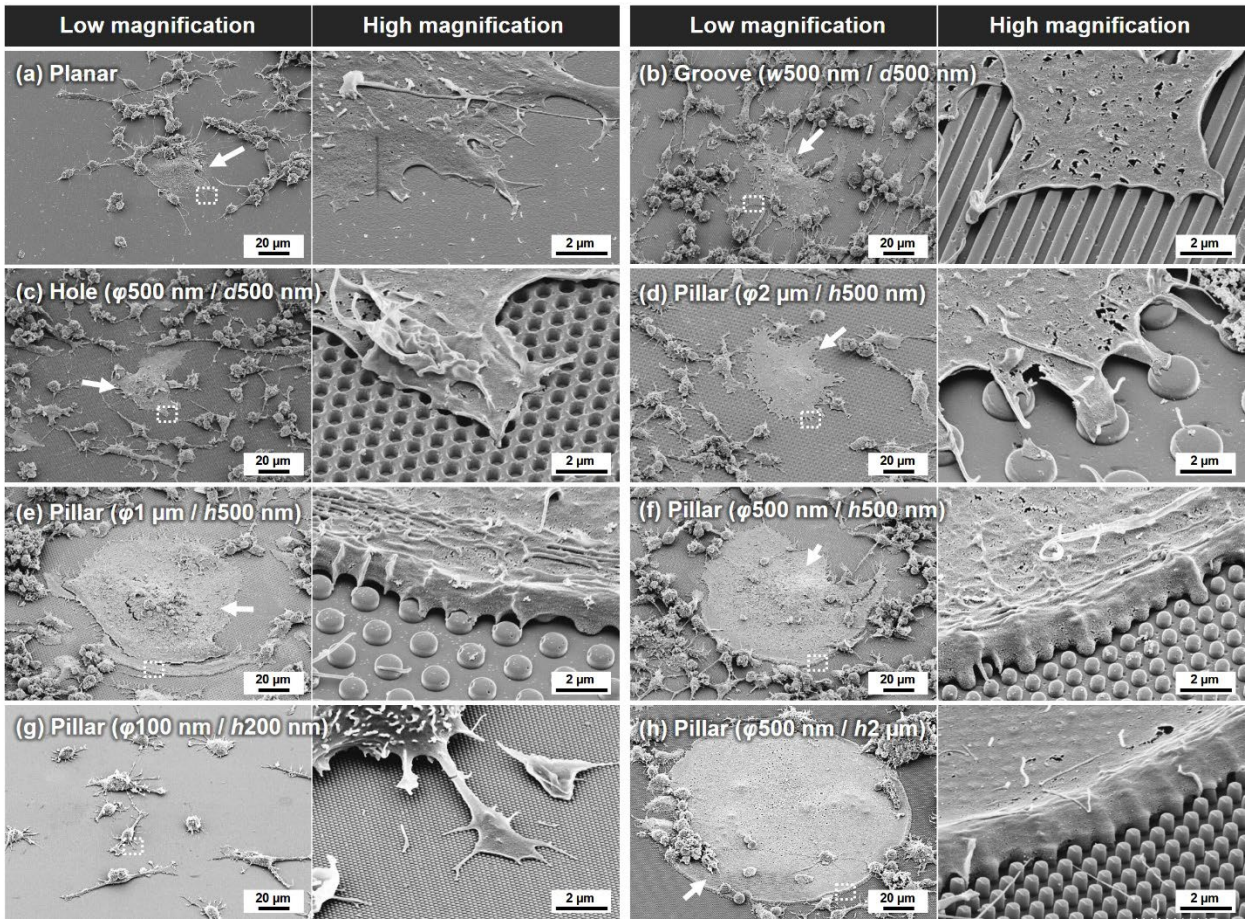
Low magnification
High magnification
Low magnification
High magnification
(a) Planar
(b) Groove (w500 nm / d500 nm)
(c) Hole (φ500 nm / d500 nm)
(d) Pillar (φ2 μm / h500 nm)
(e) Pillar (φ1 μm / h500 nm)
(f) Pillar (φ500 nm / h500 nm)
(g) Pillar (φ100 nm / h200 nm)
(h) Pillar (φ500 nm / h2 μm)
20 μm
2 μm

Figure 2

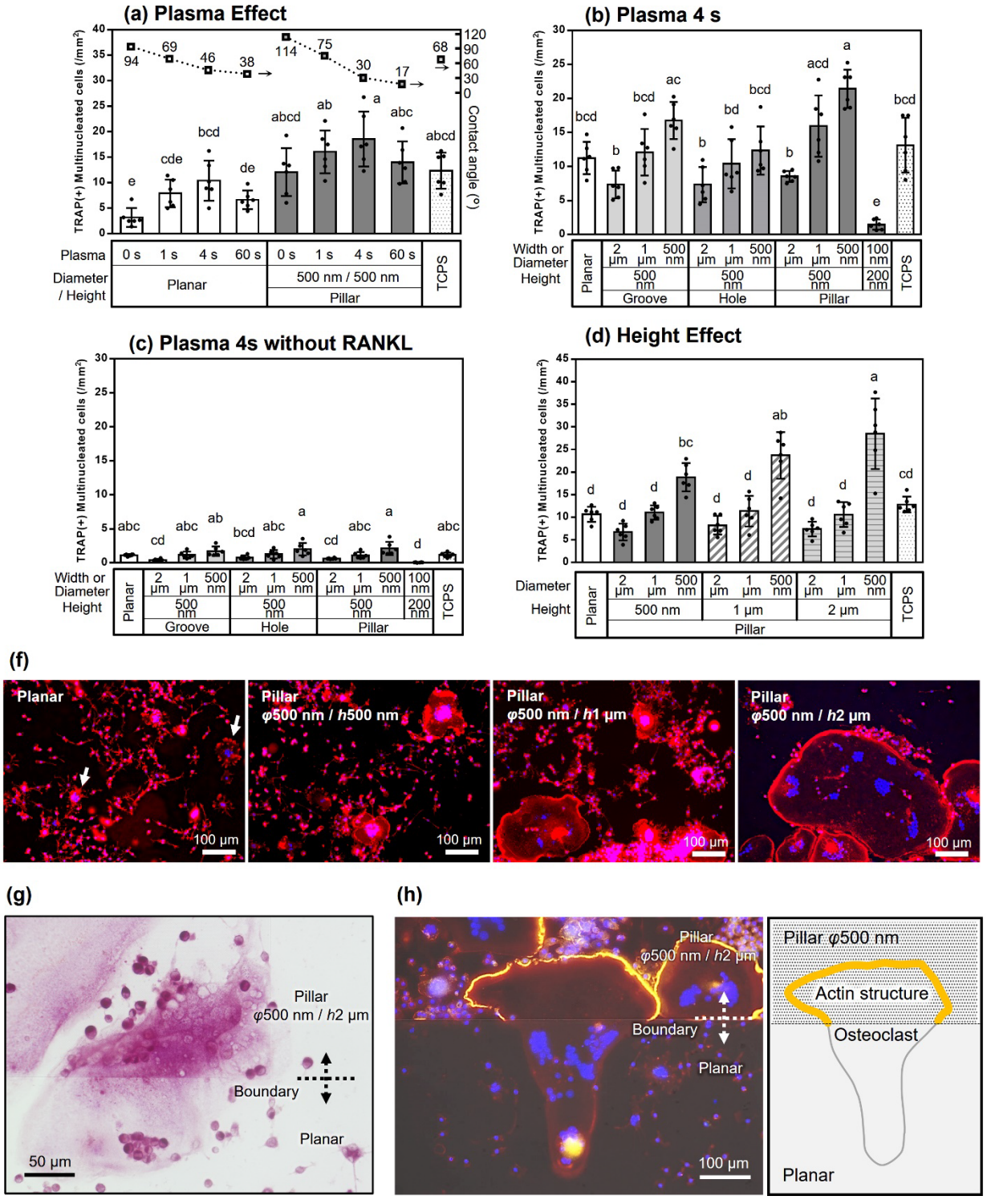
(a) Plasma Effect
TRAP(+) Multinucleated cells (/mm²)
Contact angle (°)
Plasma
Diameter / Height
0 s 1 s 4 s 60 s 0 s 1 s 4 s 60 s
Planar
500 nm / 500 nm
Pillar
TCPS
(b) Plasma 4 s
Width or Diameter Height
Planar
Groove
Hole
Pillar
(c) Plasma 4s without RANKL
(d) Height Effect
Diameter
Height
500 nm
1 μm
2 μm
(f)
Planar
Pillar φ500 nm / h500 nm
Pillar φ500 nm / h1 μm
Pillar φ500 nm / h2 μm
100 μm
(g)
Pillar φ500 nm / h2 μm
Boundary
Planar
50 μm
(h)
Pillar φ500 nm
Actin structure
Osteoclast

Figure 3

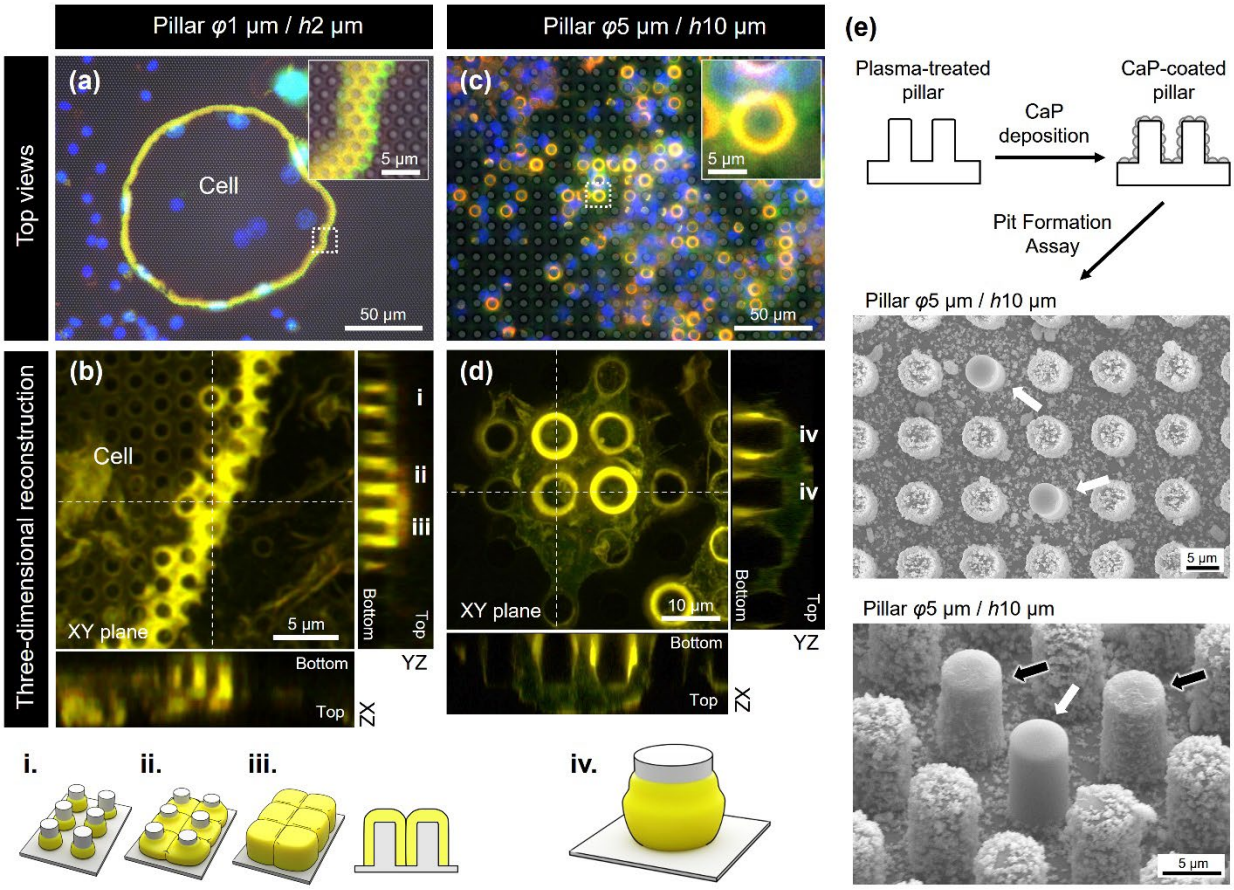

(f) Animal implantation model

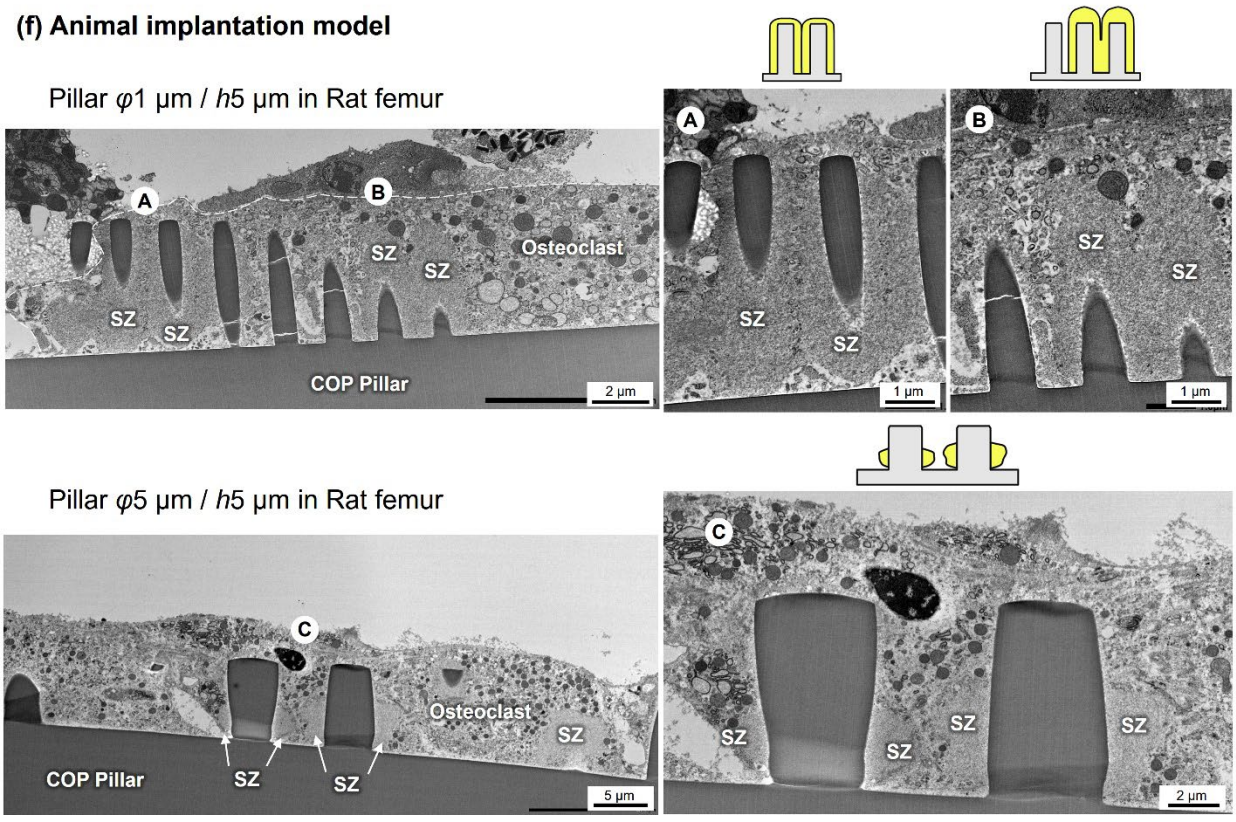

Figure 4

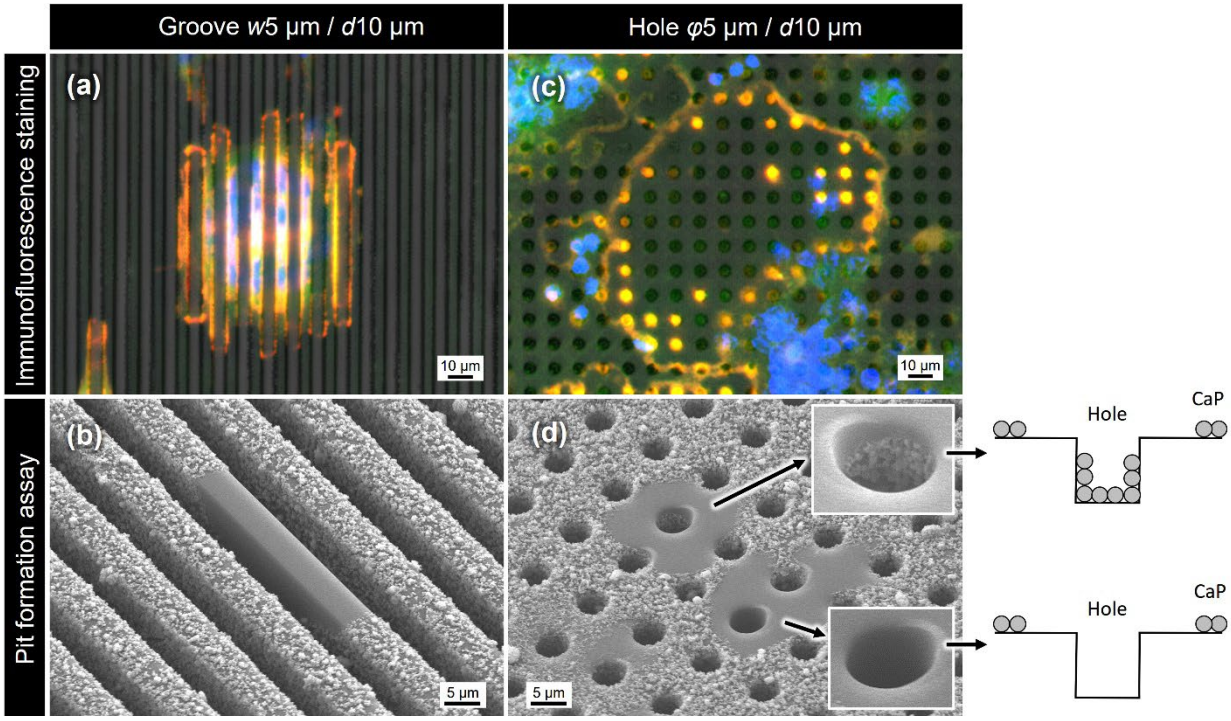

Figure 5

Electronic Supplementary Material (ESM)

S-1. Area of osteoclast-like cells cells

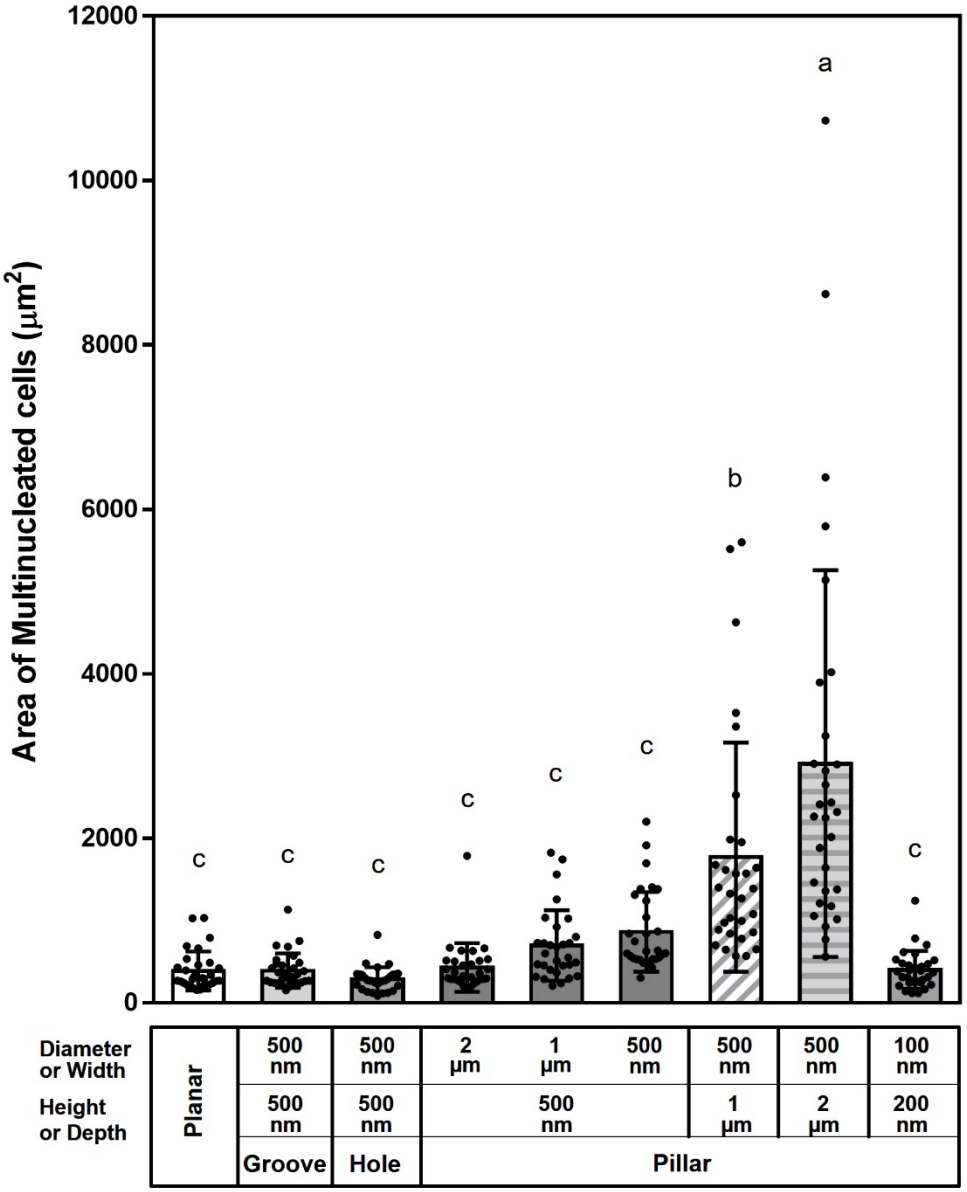

Figure S-1 Quantitative cell area analysis of osteoclast-like cells derived from RAW264.7 cells in the presence of 10 ng/mL sRANKL for 6 days. COP patterned films were treated with 4 s of plasma. Area of 30 multinucleated cells on each pattern was measured based on optical microscope photographs using ImageJ software (http://rsb.info.nih.gov/ij/). Statistical differences were assessed by one-way analysis of variance with Tukey's multiple comparison post-hoc tests. Significant differences between groups are indicated above each column with different lowercase letters ($p < 0.05$).

S-2. Effect of height or depth of the patterns on osteoclastogenesis

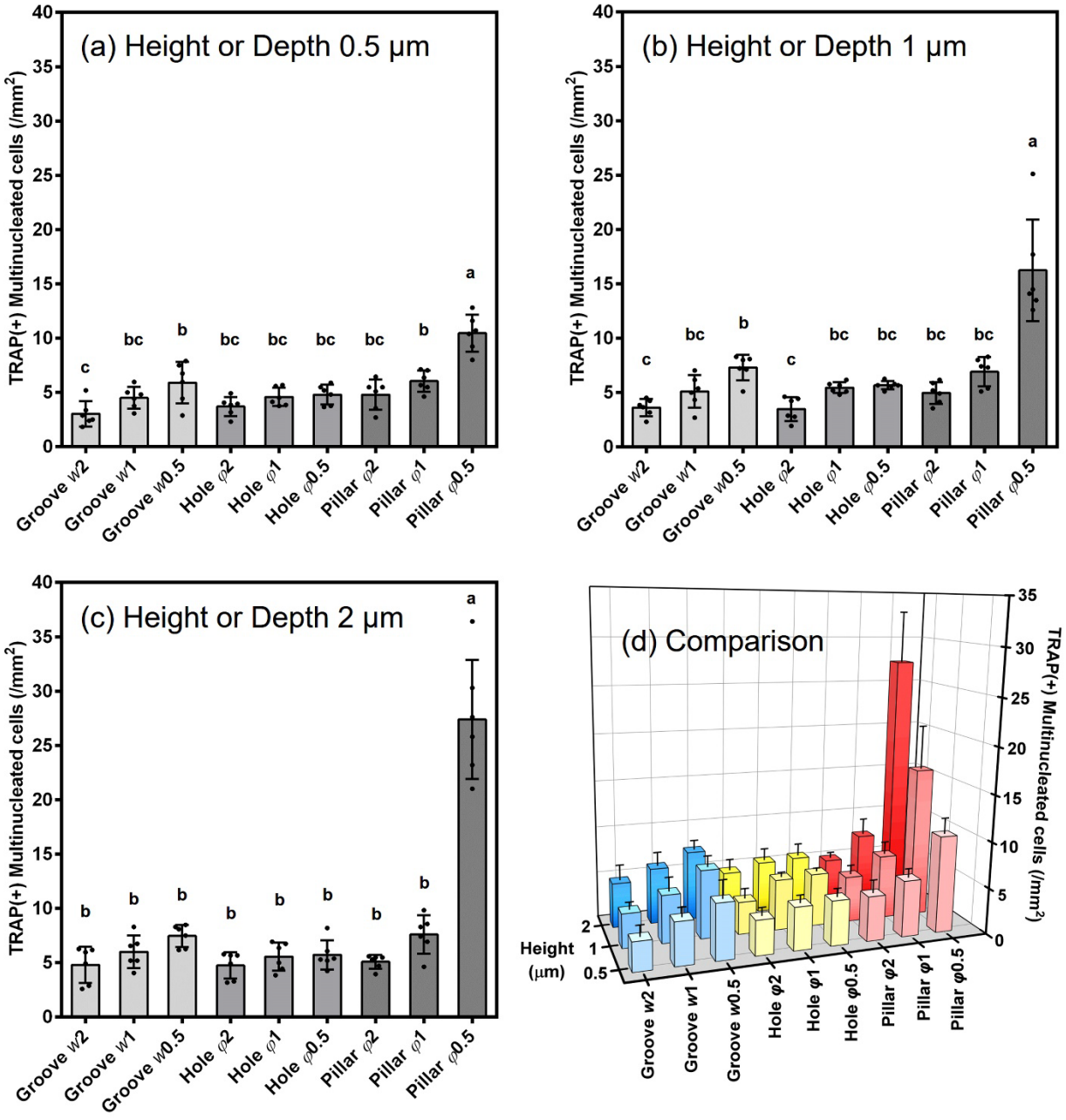

Figure S-2 The effect of pattern height or depth on the number of osteoclast-like cells derived from RAW264.7 cells in the presence of 10 ng/mL sRANKL for 6 days. COP patterned films were treated with 4 s of plasma. Bar graphs represent the number of multinucleated cells on the patterns with a height or depth of (a) 0.5, (b) 1, and (c) 2 μm. (d) Comparison of the different cellular patterns (a–c). Statistical differences were assessed by one-way analysis of variance with Tukey's

multiple comparison post-hoc tests. Significant differences between groups are indicated above each column with different lowercase letters ($p < 0.05$). Dimensions are indicated as pattern diameter (φ) or width (w).

S-3. Effect of pillars of 1 μm to 50 μm in diameter and 10 μm in height on osteoclast formation

Osteoclasts on pillars with a diameter of 10 μm or 5 μm spread and wrapped over multiple pillars. These pillars pushed up a part of the cell, transforming it into a cell with several attached pillars. Furthermore, the osteoclasts spread widely on pillars with high-aspect ratios (diameter, 1 μm; height, 10 μm). Interestingly, the lamellipodia of osteoclasts on pillars invaded the spaces between these pillars and reached their roots (Figure S-3a; iv). Figure S-3b shows that the number of osteoclasts was the highest on pillars with a diameter of 1 μm ($p < 0.05$).

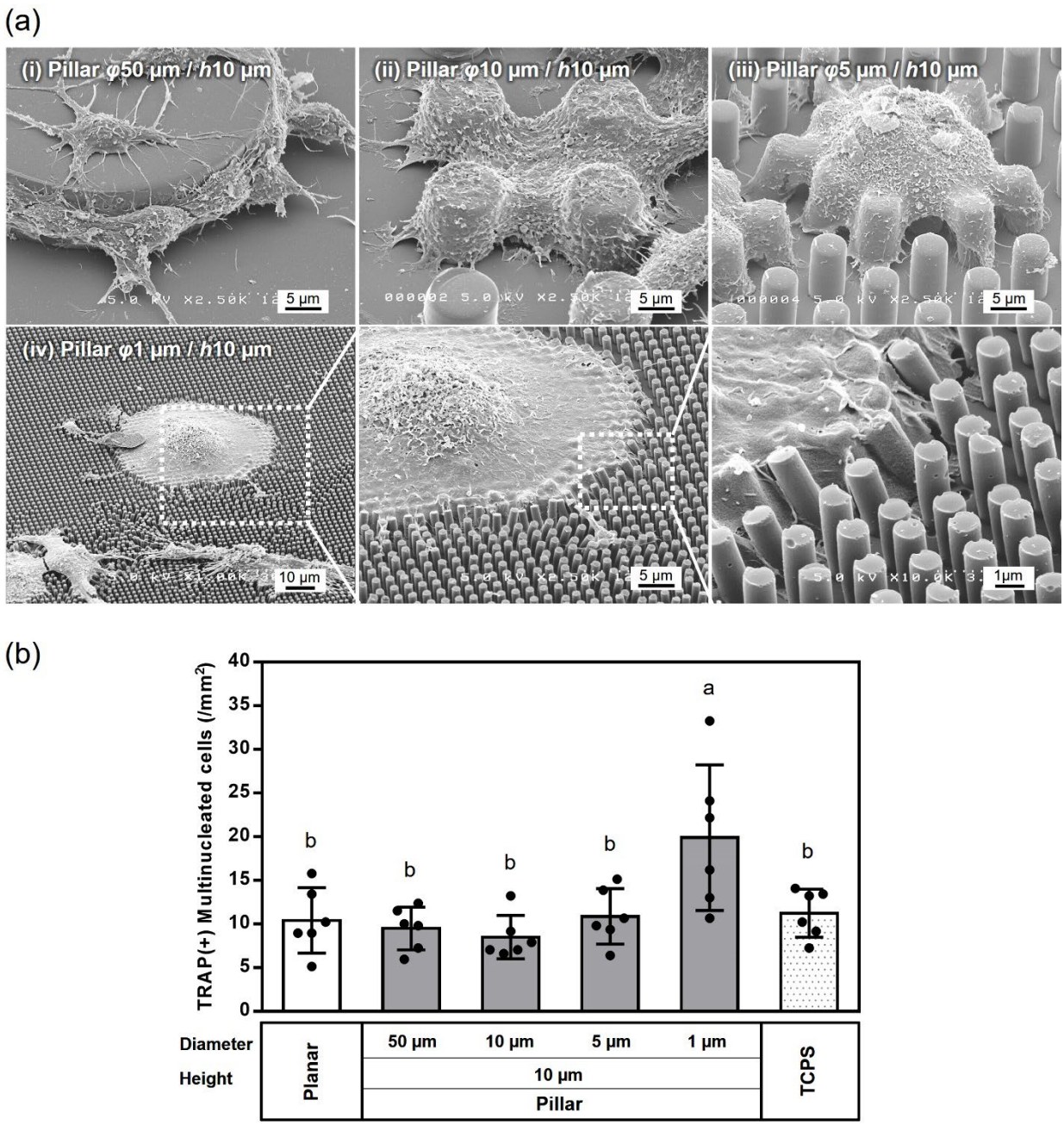

Figure S-3 Effect of pillars between 1 μm to 50 μm in diameter and 10 μm in height on osteoclast formation from RAW264.7 cells in the presence of 10 ng/ml sRANKL for 6 days. COP patterned films were treated with 4 s of plasma. (a) SEM images at a 45° tilt angle of the multinucleated osteoclast-like cells. The dotted square indicates the magnified region. (b) The number of TRAP(+)

multinucleated osteoclasts on pillars with different dimension. TCPS, tissue culture polystyrene. Dimensions are indicated as pillar diameter (φ)/height (h).

S-4. Adaptation of actin architecture to the different patterns

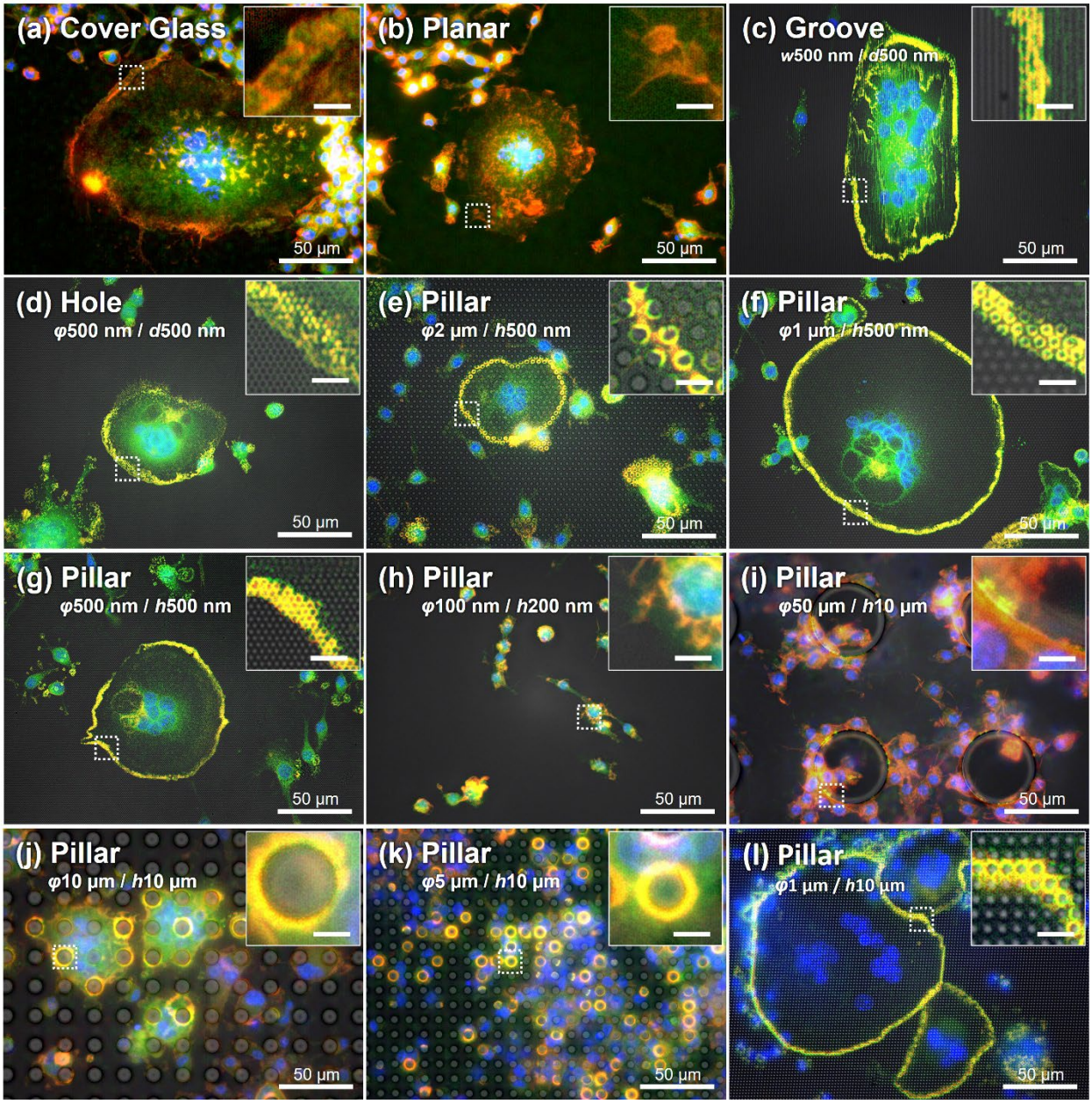

Figure S-4 Representative immunofluorescence images of multinucleated osteoclast-like cells cultured from RAW264.7 cells on different COP patterns. The cells were differentiated on 4 s

plasma-treated patterns with 10 ng/mL sRANKL for 6 days. Red staining, F-actin; green, vinculin; blue, nuclei. The three fluorescent images and bright field image were merged. Dotted squares indicate the magnified region. Scale bars = 5 μm (insets). Dimensions are indicated as pattern diameter (φ), width (w)/height (h), or depth (d).

S-5. Preparation of CaP-coated patterns

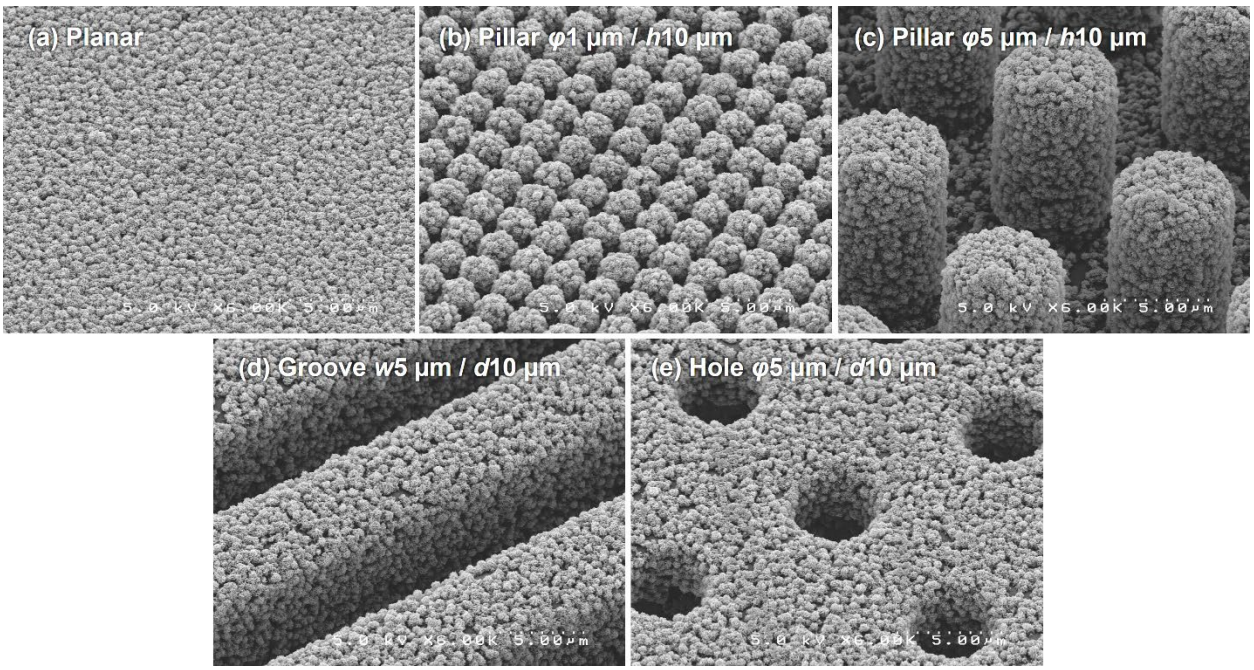

Figure S-5 SEM images of CaP-coated patterns (width or diameter/height or depth). Dimensions are indicated as pattern diameter (φ), width (w)/height (h), or depth (d).

S-6. Adaptation of actin architecture to patterns with high concentrations of sRANKL

RAW264.7 cells were differentiated in the presence of higher RANKL concentrations (100 ng/mL) to observe whether the actin architecture would be more developed.

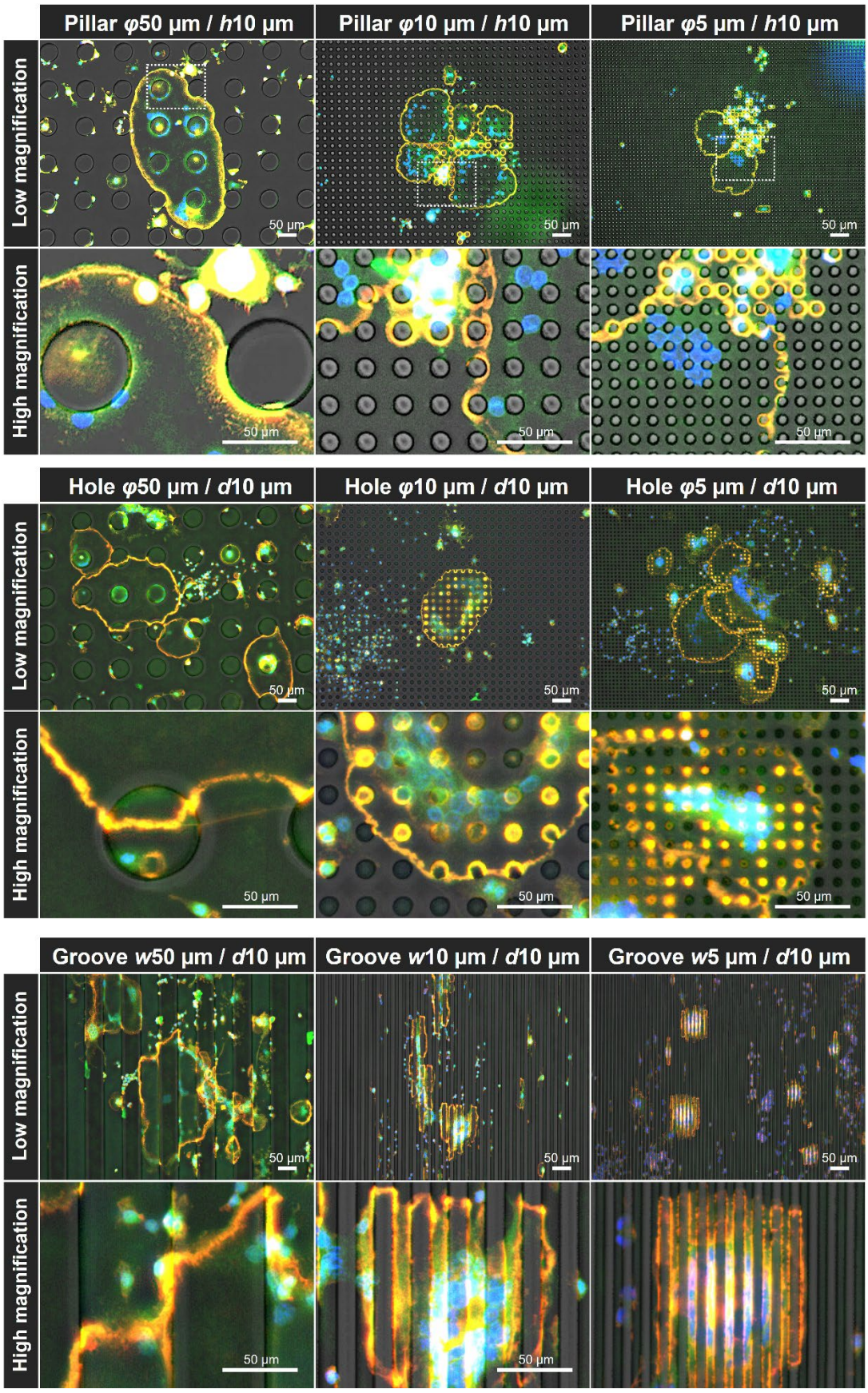
Pillar φ50 μm / h10 μm
Pillar φ10 μm / h10 μm
Pillar φ5 μm / h10 μm
Low magnification
High magnification
Hole φ50 μm / d10 μm
Hole φ10 μm / d10 μm
Hole φ5 μm / d10 μm
Groove w50 μm / d10 μm
Groove w10 μm / d10 μm
Groove w5 μm / d10 μm
50 μm

Figure S-6 Representative immunofluorescence images of multinucleated cells cultured from RAW264.7 cells on different COP patterns. The cells were differentiated on 4 s plasma-treated patterns in the presence of 100 ng/mL sRANKL for 6 days. Red staining, F-actin; green, vinculin; blue, nuclei. The three fluorescence images and bright field image were merged. Dimensions are indicated as pattern diameter (φ), width (w)/height (h), or depth (d).